Towards Understanding Feature Learning in Out-of-Distribution Generalization

Yongqiang Chen [*1] **Wei Huang** [*2] **Kaiwen Zhou** [*1] **Yatao Bian** [3] **Bo Han** [4] **James Cheng** [1]

Abstract

A common explanation for the failure of out-of-distribution (OOD) generalization is that the model trained with empirical risk minimization (ERM) learns spurious features instead of invariant features. However, several recent studies challenged this explanation and found that deep networks may have already learned sufficiently good features for OOD generalization. Despite the contradictions at first glance, we theoretically show that ERM essentially learns *both* spurious and invariant features, while ERM tends to learn spurious features faster if the spurious correlation is stronger. Moreover, when fed the ERM learned features to the OOD objectives, the invariant feature learning quality significantly affects the final OOD performance, as OOD objectives rarely learn new features. Therefore, ERM feature learning can be a *bottleneck* to OOD generalization. To alleviate the reliance, we propose **F**eature **A**ugmented **T**raining (FAT), to enforce the model to learn richer features ready for OOD generalization. FAT iteratively augments the model to learn new features while retaining the already learned features. In each round, the retention and augmentation operations are performed on different subsets of the training data that capture distinct features. Extensive experiments show that FAT effectively learns richer features thus boosting the performance of various OOD objectives.

1. Introduction

Understanding what features are learned by neural networks is crucial to understanding how they generalize to different data distributions (Rosenblatt, 1957; Shwartz-Ziv and Tishby, 2017; Shah et al., 2020; Allen-Zhu and Li, 2020). Deep networks trained with empirical risk minimization (ERM) learn highly predictive features that generalize surprisingly well to in-distribution data (Vapnik, 1991; Goodfellow et al., 2016). However, ERM also tends to learn *spurious* features such as image backgrounds (Beery et al., 2018; Geirhos et al., 2020) whose correlations with labels do not hold in the out-of-distribution (OOD) data, and suffers serious performance degeneration (Koh et al., 2021). Therefore, it is widely believed that the reason for the OOD failures of deep networks is that ERM fails to learn the desired features that have *invariant* correlations with labels across different distributions (Beery et al., 2018).

However, several recent works find that ERM-trained models have *already learned sufficiently good features* that are able to generalize to OOD data (Rosenfeld et al., 2022; Kirichenko et al., 2022; Izmailov et al., 2022). In addition, when optimizing various OOD objectives (Rojas-Carulla et al., 2018; Koyama and Yamaguchi, 2020; Parascandolo et al., 2021; Krueger et al., 2021; Pezeshki et al., 2021; Ahuja et al., 2021; Wald et al., 2021; Rame et al., 2021) that aim to capture the invariant features, there also exists an interesting phenomenon that the performance of OOD objectives largely relies on the pre-training with ERM before applying the OOD objectives (Zhang et al., 2022; Chen et al., 2022). As shown in Fig. 1(b), the number of ERM pre-training epochs *has a large influence* on the final OOD performance. These seemingly contradicting phenomena raise a challenging research question:

What features are learned by ERM and OOD objectives, respectively, and how do the learned features generalize to in-distribution and out-of-distribution data?

To answer the question, we conduct a theoretical investigation of feature learning in a two-layer CNN trained with ERM and a widely used OOD objective, IRMv1 (Arjovsky et al., 2019), respectively. We use a variation of the data models proposed in (Allen-Zhu and Li, 2020) where features can have various correlation degrees with the labels.

First, we find that ERM essentially learns *both* spurious features and invariant features (Theorem 3.1). The degrees of spurious and invariant feature learning are mostly con-

[*]Equal contribution [1]The Chinese University of Hong Kong [2]RIKEN AIP [3]Tencent AI Lab [4]Hong Kong Baptist University. Correspondence to: Yongqiang Chen <yqchen@cse.cuhk.edu.hk>, Wei Huang <wei.huang.vr@riken.jp>, Kaiwen Zhou <kwzhou@cse.cuhk.edu.hk>.

Published at the ICML 2023 Workshop on Spurious Correlations, Invariance, and Stability. Honolulu, Hawaii, USA.

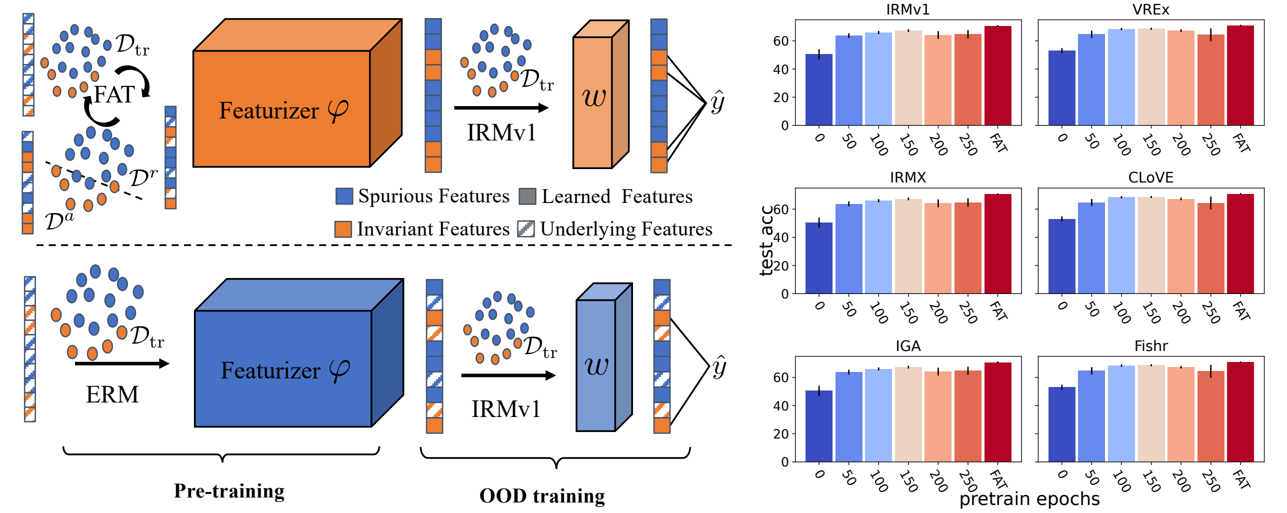

Figure 1. (a) An illustration of FAT (top row) compared to ERM (bottom row). Different colors in samples denote the corresponding dominant features. As the original data is dominated by spurious features (blue), ERM tends to learn more spurious features but limited invariant features (orange). Thus the OOD training with IRMv1 can only leverage limited invariant features and achieve limited performance. While FAT iteratively divides the training set into subsets containing distinct features by checking whether they are already learned by the model. Then FAT augments the model with new features while keep retaining the already learned features, and thus FAT learns richer features for OOD training and achieves better OOD performance. *(b)* OOD Performance vs. the number of ERM pre-training epochs. The performance of various OOD objectives largely relies on the quality of ERM-learned features. When there exist underlying useful features poorly learned by ERM, the OOD performance will be limited. FAT learns richer features and has better performance.

trolled by their correlation strengths with labels. Moreover, merely training with IRMv1 *cannot learn new* features (Theorem 3.2). Therefore, the *quality* of ERM feature learning affects the final OOD performance significantly. Hence, as the number of ERM pre-training epochs increases, the model learns invariant features better and thus the OOD performance will increase (Fig. 1). However, when ERM does not capture *all* useful features for OOD generalization, i.e., there exist some useful features poorly learned by ERM, the model can hardly learn these features during OOD training and the OOD performance will be limited. Given a limited number of pre-training steps, it could often happen due to low invariant correlation strength, the feature learning biases of ERM (Shah et al., 2020), and the neural architectures (Hermann and Lampinen, 2020). Consequently, ERM feature learning can be a *bottleneck* to OOD generalization.

To remedy the issue, we propose **F**eature **A**ugmented **T**raining (FAT), an iterative strategy to enforce the model to learn richer features. As shown in Fig. 1(a), in each round k, FAT separates the training data into two subsets according to whether the underlying features are already learned (Retention set $\mathcal{D}^r_k$) or not (Augmentation set $\mathcal{D}^a_k$), by examining whether the model yields correct ($\mathcal{D}^r_k$) or incorrect ($\mathcal{D}^a_k$) predictions for samples from the subsets, respectively. Intuitively, the augmentation sets will contain distinct features that are separated in different rounds. Then, FAT performs distributionally robust optimization (DRO) (Namkoong and Duchi, 2016; Zhang et al., 2022) on $\{\mathcal{D}^a_k, \mathcal{D}^r_k\}$ to *augment* the model to learn new features. Meanwhile, FAT also *retains* the already learned features via ERM on $\{\mathcal{D}^r_k\}$. FAT terminates when the model cannot learn any new predictive features from the augmentation subsets (Algorithm 1).

We conduct extensive experiments on both COLOREDMNIST and 6 datasets from the challenging benchmark, WILDS to verify the effectiveness of FAT (Sec. G).

2. Preliminaries and Problem Definition

We leave the full introduction of background and notations to Appendix B and C, due to space constraints.

Notations. We use bold-faced letters for vectors and matrices otherwise for scalar. We use $\|\cdot\|_2$ to denote the Euclidean norm of a vector or the spectral norm of a matrix. $\mathbf{I}_d$ refers to the identity matrix with a dimension of $\mathbb{R}^{d\times d}$. Our data model $\mathcal{D} = \{\mathbf{x}_i, y_i\}_{i=1}^n$ is adapted from (Allen-Zhu and Li, 2020) and characterizes each data point $\mathbf{x}_i$ as invariant and spurious feature patches (Kamath et al., 2021).

Definition 2.1. $\mathcal{D} = \{\mathcal{D}_e\}_{e\in\mathcal{E}_{\text{all}}}$ is composed of multiple subsets $\mathcal{D}_e$ from different environments $e \in \mathcal{E}_{\text{all}}$, where each $\mathcal{D}_e = \{(\mathbf{x}^e_i, y^e_i)\}_{i=1}^{n_e}$ is composed of i.i.d. samples $(\mathbf{x}^e_i, y^e_i)$. Each data $(\mathbf{x}^e, y^e) \in \mathcal{D}_e$ with $\mathbf{x}^e \in \mathbb{R}^{2d}$ and $y^e \in \{-1, 1\}$ is generated as follows: (a) Sample $y^e \in \{-1, 1\}$ uniformly; (b) Given y^e, each input $\mathbf{x}^e = [\mathbf{x}^e_1, \mathbf{x}^e_2]$ contains a feature patch $\mathbf{x}_1$ and a noise patch $\mathbf{x}_2$ sampled as:

$$\mathbf{x}_1 = y \cdot \text{Rad}(\alpha) \cdot \mathbf{v}_1 + y \cdot \text{Rad}(\beta) \cdot \mathbf{v}_2 \quad \mathbf{x}_2 = \boldsymbol{\xi}$$

where $\text{Rad}(\delta)$ is a random variable taking value -1 with probability δ and $+1$ with probability $1 - \delta$, $\mathbf{v}_1 =$

$[1, 0, \dots 0]^\top$ and $\mathbf{v}_2 = [0, 1, 0, \dots 0]^\top$; (c) A noise vector $\boldsymbol{\xi}$ is sampled from $\mathcal{N}(\mathbf{0}, \sigma_p^2 \cdot (\mathbf{I}_d - \mathbf{v}_1\mathbf{v}_1^\top - \mathbf{v}_2\mathbf{v}_2^\top))$;

Definition 2.1 is inspired by image classification, where the inputs consist of different patches. Each environment is denoted as $\mathcal{E}_\alpha = \{(\alpha, \beta_e)\}$, where $\mathbf{v}_1$ is the invariant feature as α is fixed while $\mathbf{v}_2$ is the spurious as β_e varies across e.

CNN model. We consider training a two-layer convolutional neural network with a hidden layer width of m. The filters are applied to $\mathbf{x}_1$, $\mathbf{x}_2$, respectively,[1] and the second layer parameters of the network are fixed as $\frac{1}{m}$ and $-\frac{1}{m}$, respectively. Then the network can be written as $f(\mathbf{W}, \mathbf{x}) = F_{+1}(\mathbf{W}_{+1}, \mathbf{x}) - F_{-1}(\mathbf{W}_{-1}, \mathbf{x})$, where $F_{+1}(\mathbf{W}_{+1}, \mathbf{x})$ and $F_{-1}(\mathbf{W}_{-1}, \mathbf{x})$ are defined as follows:

$$F_j(\mathbf{W}_j, \mathbf{x}) = \frac{1}{m}\sum_{r=1}^{m}\left[\sigma(\mathbf{w}_{j,r}^\top \mathbf{x}_1) + \sigma(\mathbf{w}_{j,r}^\top \mathbf{x}_2)\right], \quad (1)$$

where $\sigma(x)$ is the activation function. We focus on linear activation $\sigma(x) = x$ since it is sufficient to observe the desired feature learning behaviors of ERM and OOD objectives.[2]

ERM objective. We train the CNN model by minimizing the empirical cross-entropy loss function:

$$L_S(\mathbf{W}) = \sum_{e \in \mathcal{E}_{\text{tr}}} \frac{1}{n_e}\sum_{i=1}^{n_e} \ell(y_i^e \cdot f(\mathbf{W}, \mathbf{x}_i^e)), \quad (2)$$

where $\ell(z) = \log(1 + \exp(-z))$ and $\{\mathcal{D}_e\}_{e \in \mathcal{E}_{\text{tr}}} = \{\{\mathbf{x}_i^e, y_i^e\}_{i=1}^{n_e}\}_{e \in \mathcal{E}_{\text{tr}}}$ is the trainset with $\sum_{e \in \mathcal{E}_{\text{tr}}} n_e = n$.

OOD objective. Since we are interested in cases where the OOD objective succeeds in learning the invariant features. In the discussion below, without loss of generality, we study one of the most widely discussed OOD objective, IRMv1 objective (Arjovsky et al., 2019), and the data model where IRMv1 succeeds. Given the convolutional neural network (Eq. 1) and logistic loss (Eq. 2), IRMv1 can be written as

$$L_{\text{IRMv1}}(\mathbf{W}) = \sum_{e \in \mathcal{E}_{\text{tr}}} \frac{1}{n_e}\sum_{i=1}^{n_e} \ell\left(y_i^e \cdot f(\mathbf{W}, \mathbf{x}_i^e)\right) + \sum_{e \in \mathcal{E}_{\text{tr}}} \frac{\lambda}{n_e^2}\left(\sum_{i=1}^{n_e} \ell_i' \cdot y_i^e \cdot f(\mathbf{W}, \mathbf{x}_i^e)\right)^2, \quad (3)$$

where ${\ell'}_i^e = \ell'(y_i^e \cdot f(\mathbf{W}, \mathbf{x}_i^e)) = -\frac{\exp(-y_i^e \cdot f(\mathbf{W}, \mathbf{x}_i^e))}{1+\exp(-y_i^e \cdot f(\mathbf{W}, \mathbf{x}_i^e))}$. Due to the complexity of IRMv1, in the analysis below, we introduce C_{IRMv1}^e for the ease of expressions. Specifically,

$$C_{\text{IRMv1}}^e \triangleq \frac{1}{n_e}\sum_{i=1}^{n_e} \ell'\left(y_i^e \hat{y}_i^e\right) \cdot y_i^e \hat{y}_i^e,$$

where $\hat{y}_i^e \triangleq f(\mathbf{W}, \mathbf{x}_i^e)$. The convergence of C_{IRMv1} indicates the convergence of IRMv1 penalty. Furthermore, $\gamma_{j,r,1} \approx \langle \mathbf{w}_{j,r}, \mathbf{v}_1 \rangle$ and $\gamma_{j,r,2} \approx \langle \mathbf{w}_{j,r}, \mathbf{v}_2 \rangle$ respectively denote the degrees of invariant and spurious feature learning. For ease of understanding, in the discussion below, we will denote $\gamma_{j,r,1}$ and $\gamma_{j,r,2}$ as $\gamma_{j,r}^{inv}$ and $\gamma_{j,r}^{spu}$, respectively.

3. Feature Learning in OOD Generalization

ERM Feature Learning. We first study the feature learning process of ERM objective. We consider a two training environments setup $\mathcal{E}_{tr} = \{(\alpha, \beta_1), (\alpha, \beta_2)\}$ where the signal of invariant feature is weaker than the average of spurious signals (i.e., $\alpha > \frac{\beta_1+\beta_2}{2}$), which corresponds to Figure 2.

Theorem 3.1. *(Informal) For $\rho > 0$, let $\underline{n} \triangleq \min_{e \in \mathcal{E}_{tr}} n_e$. Suppose that we run T iterations of GD for the ERM objective. With sufficiently large $\underline{n}$, assuming that (i) $\alpha, \beta_1, \beta_2 < \frac{1}{2}$, and (ii) $\alpha > \frac{\beta_1+\beta_2}{2}$, with properly chosen σ_0^2 and σ_p^2, there exists a constant η, such that with probability at least $1 - 2\rho$, both invariant and spurious features are converging and the increment of the spurious feature is larger than that of the invariant feature at any iteration $t \in \{0, \dots, T-1\}$.*

The formal statement of this theorem and its proof are given in Appendix D.2. Corresponding to Figure 2(b), Theorem 3.1 explains the seemingly contradicting observations of ERM feature learning. On the one hand, ERM fails since it learns the spurious features at a higher speed, when spurious correlations are stronger than invariant correlations. Although spurious feature learning effectively reduces the empirical risk, the learned features cannot generalize to OOD data where the correlations between spurious features and labels no longer hold (Beery et al., 2018). On the other hand, the invariant feature learning also happens, even when the spurious correlations are strong, so long as the invariant feature has a non-trivial correlation strength with the labels. Therefore, simply re-training a classifier based on a subset of unbiased data on top of the ERM-trained featurizer achieves impressive OOD performance (Rosenfeld et al., 2022; Kirichenko et al., 2022; Izmailov et al., 2022).

IRM Feature Learning. We then study IRMv1 training from scratch (w/o pre-training).

Theorem 3.2. *(Informal) Consider training a CNN model with the same data as in Theorem 3.1, define $\mathbf{c}(t) \triangleq \left[C_{IRMv1}^1(\mathbf{W}, t), C_{IRMv1}^2(\mathbf{W}, t), \cdots, C_{IRMv1}^{|\mathcal{E}_{tr}|}(\mathbf{W}, t)\right]$. Under certain conditions, with probability at least $1 - \delta$, after training time $T = \Omega\left(\frac{\log(1/\epsilon)}{\eta\lambda\lambda_0}\right)$, we have $\|\mathbf{c}(T)\|_2 \le \epsilon$, $\gamma_{j,r,1}(T) = o_d(1)$, $\gamma_{j,r,2}(T) = o_d(1)$.*

The formal statement of this theorem proof are given in Appendix D.3. Intuitively, Theorem 3.2 implies that, when a heavy regularization of IRMv1 is applied, the model will not learn any features, corresponding to Figure 2(d). Then, what

[1] When e is not explicitly considered, we will omit it for clarity.

[2] It is also due to the complexity of IRMv1 dynamics. To the best of our knowledge, we are the first to study IRMv1 dynamics.

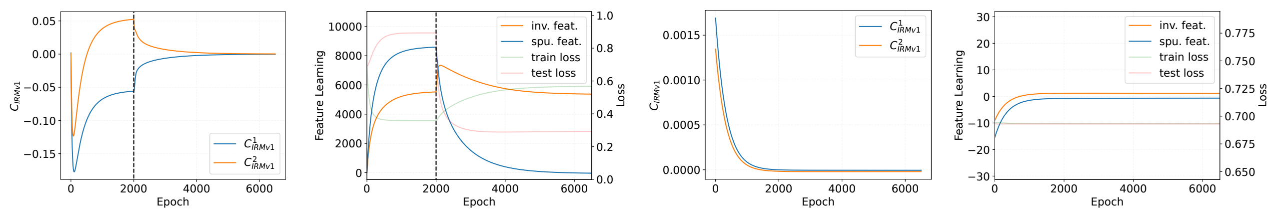

(a) C_{IRMv1}, w/ PT (b) FL, w/ PT (c) C_{IRMv1}, w/o PT (d) FL, w/o PT

Figure 2. The convergences of C_{IRMv1} and feature learning coefficients (FL) with or without ERM pre-training (PT). The training environments are $\mathcal{E}_{tr} = \{(0.25, 0.1), (0.25, 0.2)\}$. The black dashed line indicates the end of pre-training. Details are in Appendix D.1.

would happen when given a properly pre-trained network?

Proposition 3.3. *Given the same setting as Theorem 3.1, ERM pre-training converges at t_1, $\delta > 0$, and $n > C\log(1/\delta)$, with C being a positive constant, then with a high probability at least $1-\delta$, we have $\sum_e C^e_{IRMv1}(t_1) = 0$, $\gamma^{inv}_{j,r}(t_1+1) > \gamma^{inv}_{j,r}(t_1)$, and $\gamma^{spu}_{j,r}(t_1+1) < \gamma^{spu}_{j,r}(t_1)$.*

The proof is given in Appendix D.4. Proposition 3.3 demonstrates that with sufficient ERM pre-training, IRMv1 can enhance the learning of invariant features while suppressing the learning of spurious features, which is verified in Figure 2(b) and 2(a). Thus, when given the initialization with better learned invariant features, i.e., longer ERM pre-training epochs, IRMv1 improves the invariant feature better. Proposition 3.3 explains why the OOD performance highly depends on the ERM pre-training (Chen et al., 2022).

Limitations of ERM Feature Learning. The remaining curious question is, given a poorly learned invariant feature, will IRMv1 still improve it? In practice, there often exist some invariant features that are not properly learned by ERM. For example, in Def. 2.1 when the invariant correlation is much weaker than the spurious correlation, given a limited number of training steps, the spurious feature learning can dominate the invariant feature learning. Besides, when considering other factors such as the inductive biases of ERM (Shah et al., 2020) or neural architecture (Hermann and Lampinen, 2020), it is more likely that there exist invariant features not properly learned. Then:

Corollary 3.4. *Consider training the CNN with the data generated from Def. 2.1, suppose that $\gamma^{inv}_{j,r}(t_1) = o(1)$ and $\gamma^{spu}_{j,r}(t_1) = \Theta(1)$ at the end of ERM pre-training t_1. Suppose that $\delta > 0$, and $n > C\log(1/\delta)$, with C being a positive constant, then with a high probability at least $1-\delta$, we have $\gamma^{inv}_{j,r}(t_1+1) < \gamma^{inv}_{j,r}(t_1)$.*

Corollary 3.4 shows that IRMv1 requires sufficiently well-learned features for OOD generalization. It is also consistent with the results in Fig. 2(b), 2(c), and Fig. 1, where all the OOD objectives perform comparably to random guesses.

Improving Feature Learning for OOD Generalization. Previous results imply that the model is expected to learn all potentially useful features during the pre-training in order to achieve the optimal OOD performance. To this end, we propose **F**eature **A**ugmented **T**raining (FAT), that adopts an iterative data-centric strategy to enforce the model to learn all useful features directly. We briefly introduce FAT below and leave more details in Appendix E.

Intuitively, the potentially useful features presented in the training data are features that have non-trivial correlations with labels. Moreover, the invariance principle assumes that the training data comes from different environments (Arjovsky et al., 2019), where each set of features can only dominate the correlations with labels in a *subset* of data. Therefore, it is possible to differentiate the distinct sets of useful features entangled in the trainset into distinct subsets.

The intuition motivates an iterative feature learning algorithm, i.e., FAT, that identifies the subsets and explores new features by multiple rounds. In round k, FAT first identifies the subset that contains the already learned features by collecting the data points where f yields the correct prediction, denoted as G^r_k, and the subset that contains the other samples as G^a_k. Given a grouped datasets $G = \{G^r, G^a\}$ with $2k-1$ groups, where $G^a = \{\mathcal{D}^a_i\}_{i=0}^{k-1}$ and $G^r = \{\mathcal{D}^r_i\}_{i=1}^{k-1}$ (notice that $\mathcal{D}^r_0$ is the empty set), FAT performs distributionally robust optimization (DRO) (Namkoong and Duchi, 2016) on G^a to explore new features that have not been learned in previous rounds. Meanwhile, FAT also needs to *retain* the already learned features by ERM at G^r, as

$$\ell_{\text{FAT}} = \max_{\mathcal{D}^a_i \in G^a} \ell_{\mathcal{D}^a_i}(w_k \circ \varphi) + \lambda \cdot \sum_{\mathcal{D}^r_i \in G^r} \ell_{\mathcal{D}^r_i}(w_i \circ \varphi), \quad (4)$$

where $\ell_{\mathcal{D}_i}(w \circ \varphi)$ is the empirical risk of $w \circ \varphi$ at $\mathcal{D}_i$, and $\{w_i | 1 \leq i \leq k-1\}$ are the historical classifiers.

Empirical verification. We verified the effectiveness of FAT in Fig. 1 and also in COLOREDMNIST and challenging benchmark WILDS as shown in Appendix G.

4. Conclusions

In this paper, we found that ERM learns both invariant and spurious features when OOD objectives rarely learn new features. Thus, the features learned in the ERM pre-training can greatly influence the final OOD performance. Having learned the limitations of ERM pre-training, we proposed FAT to learn all potentially useful features. Extensive experimental results verified the superiority of FAT.

Acknowledgements

We thank the reviewers for their valuable comments. This work was supported by CUHK direct grant 4055146. BH were supported by the NSFC Young Scientists Fund No. 62006202, Guangdong Basic and Applied Basic Research Foundation No. 2022A1515011652, RGC Early Career Scheme No. 22200720, and Tencent AI Lab Rhino-Bird Gift Fund.

References

K. Ahuja, E. Caballero, D. Zhang, J.-C. Gagnon-Audet, Y. Bengio, I. Mitliagkas, and I. Rish. Invariance principle meets information bottleneck for out-of-distribution generalization. In *Advances in Neural Information Processing Systems*, 2021.

Z. Allen-Zhu and Y. Li. Towards understanding ensemble, knowledge distillation and self-distillation in deep learning. *arXiv preprint arXiv:2012.09816*, 2020.

A. Andreassen, Y. Bahri, B. Neyshabur, and R. Roelofs. The evolution of out-of-distribution robustness throughout fine-tuning. *arXiv preprint arXiv:2106.15831*, 2021.

M. Arjovsky, L. Bottou, I. Gulrajani, and D. Lopez-Paz. Invariant risk minimization. *arXiv preprint arXiv:1907.02893*, 2019.

D. Arpit, H. Wang, Y. Zhou, and C. Xiong. Ensemble of averages: Improving model selection and boosting performance in domain generalization. In *Advances in Neural Information Processing Systems*, 2022.

P. Bándi, O. Geessink, Q. Manson, M. V. Dijk, M. Balkenhol, M. Hermsen, B. E. Bejnordi, B. Lee, K. Paeng, A. Zhong, Q. Li, F. G. Zanjani, S. Zinger, K. Fukuta, D. Komura, V. Ovtcharov, S. Cheng, S. Zeng, J. Thagaard, A. B. Dahl, H. Lin, H. Chen, L. Jacobsson, M. Hedlund, M. Çetin, E. Halici, H. Jackson, R. Chen, F. Both, J. Franke, H. Küsters-Vandevelde, W. Vreuls, P. Bult, B. van Ginneken, J. van der Laak, and G. Litjens. From detection of individual metastases to classification of lymph node status at the patient level: The CAMELYON17 challenge. *IEEE Trans. Medical Imaging*, 38 (2):550–560, 2019.

S. Beery, G. V. Horn, and P. Perona. Recognition in terra incognita. In *Computer Vision European Conference, Part XVI*, pages 472–489, 2018.

S. Beery, E. Cole, and A. Gjoka. The iwildcam 2020 competition dataset. *arXiv preprint arXiv:2004.10340*, 2020.

D. Borkan, L. Dixon, J. Sorensen, N. Thain, and L. Vasserman. Nuanced metrics for measuring unintended bias with real data for text classification. In *Companion of The 2019 World Wide Web Conference*, pages 491–500, 2019.

A. Brutzkus, A. Globerson, E. Malach, and S. Shalev-Shwartz. SGD learns over-parameterized networks that provably generalize on linearly separable data. In *International Conference on Learning Representations*, 2018.

Y. Cao, Z. Chen, M. Belkin, and Q. Gu. Benign overfitting in two-layer convolutional neural networks. In *Advances in Neural Information Processing Systems*, 2022.

Y. Chen, K. Zhou, Y. Bian, B. Xie, K. Ma, Y. Zhang, H. Yang, B. Han, and J. Cheng. Pareto invariant risk minimization. *arXiv preprint arXiv:2206.07766*, 2022.

G. A. Christie, N. Fendley, J. Wilson, and R. Mukherjee. Functional map of the world. In *IEEE Conference on Computer Vision and Pattern Recognition*, pages 6172–6180, 2018.

N. Elhage, T. Hume, C. Olsson, N. Schiefer, T. Henighan, S. Kravec, Z. Hatfield-Dodds, R. Lasenby, D. Drain, C. Chen, R. Grosse, S. McCandlish, J. Kaplan, D. Amodei, M. Wattenberg, and C. Olah. Toy models of superposition. *arXiv preprint arXiv:2209.10652*, 2022.

S. Frei, Y. Cao, and Q. Gu. Provable generalization of sgd-trained neural networks of any width in the presence of adversarial label noise. In *International Conference on Machine Learning*, pages 3427–3438, 2021.

R. Geirhos, J. Jacobsen, C. Michaelis, R. S. Zemel, W. Brendel, M. Bethge, and F. A. Wichmann. Shortcut learning in deep neural networks. *Nature Machine Intelligence*, 2 (11):665–673, 2020.

I. Goodfellow, Y. Bengio, and A. Courville. *Deep Learning*. MIT Press, 2016. http://www.deeplearningbook.org.

I. Gulrajani and D. Lopez-Paz. In search of lost domain generalization. In *International Conference on Learning Representations*, 2021.

A. Gupta, N. Saunshi, D. Yu, K. Lyu, and S. Arora. New definitions and evaluations for saliency methods: Staying intrinsic and sound, 2022.

K. He, X. Zhang, S. Ren, and J. Sun. Deep residual learning for image recognition. In *IEEE Conference on Computer Vision and Pattern Recognition*, pages 770–778, 2016.

K. Hermann and A. Lampinen. What shapes feature representations? exploring datasets, architectures, and training. In *Advances in Neural Information Processing Systems*, pages 9995–10006, 2020.

G. Huang, Z. Liu, L. van der Maaten, and K. Q. Weinberger. Densely connected convolutional networks. In *IEEE Conference on Computer Vision and Pattern Recognition*, pages 2261–2269, 2017.

P. Izmailov, P. Kirichenko, N. Gruver, and A. G. Wilson. On feature learning in the presence of spurious correlations. In *Advances in Neural Information Processing Systems*, 2022.

P. Kamath, A. Tangella, D. Sutherland, and N. Srebro. Does invariant risk minimization capture invariance? In *International Conference on Artificial Intelligence and Statistics*, pages 4069–4077, 2021.

D. P. Kingma and J. Ba. Adam: A method for stochastic optimization. In *International Conference on Learning Representations*, 2015.

P. Kirichenko, P. Izmailov, and A. G. Wilson. Last layer re-training is sufficient for robustness to spurious correlations. *arXiv preprint arXiv:2204.02937*, 2022.

P. W. Koh, S. Sagawa, H. Marklund, S. M. Xie, M. Zhang, A. Balsubramani, W. Hu, M. Yasunaga, R. L. Phillips, I. Gao, T. Lee, E. David, I. Stavness, W. Guo, B. Earnshaw, I. Haque, S. M. Beery, J. Leskovec, A. Kundaje, E. Pierson, S. Levine, C. Finn, and P. Liang. WILDS: A benchmark of in-the-wild distribution shifts. In *International Conference on Machine Learning,*, pages 5637–5664, 2021.

M. Koyama and S. Yamaguchi. Out-of-distribution generalization with maximal invariant predictor. *arXiv preprint arXiv:2008.01883*, 2020.

D. Krueger, E. Caballero, J. Jacobsen, A. Zhang, J. Binas, D. Zhang, R. L. Priol, and A. C. Courville. Out-of-distribution generalization via risk extrapolation (rex). In *International Conference on Machine Learning*, pages 5815–5826, 2021.

A. Kumar, A. Raghunathan, R. M. Jones, T. Ma, and P. Liang. Fine-tuning can distort pretrained features and underperform out-of-distribution. In *International Conference on Learning Representations*, 2022a.

A. Kumar, A. Raghunathan, R. M. Jones, T. Ma, and P. Liang. Fine-tuning can distort pretrained features and underperform out-of-distribution. In *International Conference on Learning Representations*, 2022b.

J. P. Miller, R. Taori, A. Raghunathan, S. Sagawa, P. W. Koh, V. Shankar, P. Liang, Y. Carmon, and L. Schmidt. Accuracy on the line: on the strong correlation between out-of-distribution and in-distribution generalization. In *International Conference on Machine Learning*, pages 7721–7735, 2021.

H. Naganuma, K. Ahuja, I. Mitliagkas, S. Takagi, T. Motokawa, R. Yokota, K. Ishikawa, and I. Sato. Empirical study on optimizer selection for out-of-distribution generalization. *arXiv preprint arXiv:2211.08583*, 2022.

H. Namkoong and J. C. Duchi. Stochastic gradient methods for distributionally robust optimization with f-divergences. In *Advances in Neural Information Processing Systems*, pages 2208–2216, 2016.

J. Ni, J. Li, and J. McAuley. Justifying recommendations using distantly-labeled reviews and fine-grained aspects. In *Conference on Empirical Methods in Natural Language Processing and International Joint Conference on Natural Language Processing*, pages 188–197, 2019.

G. Parascandolo, A. Neitz, A. Orvieto, L. Gresele, and B. Schölkopf. Learning explanations that are hard to vary. In *International Conference on Learning Representations*, 2021.

A. Paszke, S. Gross, F. Massa, A. Lerer, J. Bradbury, G. Chanan, T. Killeen, Z. Lin, N. Gimelshein, L. Antiga, A. Desmaison, A. Kopf, E. Yang, Z. DeVito, M. Raison, A. Tejani, S. Chilamkurthy, B. Steiner, L. Fang, J. Bai, and S. Chintala. Pytorch: An imperative style, high-performance deep learning library. In *Advances in Neural Information Processing Systems*, pages 8024–8035, 2019.

M. Pezeshki, S. Kaba, Y. Bengio, A. C. Courville, D. Precup, and G. Lajoie. Gradient starvation: A learning proclivity in neural networks. In *Advances in Neural Information Processing Systems*, pages 1256–1272, 2021.

A. Rame, C. Dancette, and M. Cord. Fishr: Invariant gradient variances for out-of-distribution generalization. *arXiv preprint arXiv:2109.02934*, 2021.

A. Ramé, K. Ahuja, J. Zhang, M. Cord, L. Bottou, and D. Lopez-Paz. Model ratatouille: Recycling diverse models for out-of-distribution generalization. *arXiv preprint arXiv:2212.10445*, 2022.

A. Rame, M. Kirchmeyer, T. Rahier, A. Rakotomamonjy, patrick gallinari, and M. Cord. Diverse weight averaging for out-of-distribution generalization. In *Advances in Neural Information Processing Systems*, 2022.

M. Rojas-Carulla, B. Schölkopf, R. Turner, and J. Peters. Invariant models for causal transfer learning. *Journal of Machine Learning Research*, 19(36):1–34, 2018.

F. Rosenblatt. The perceptron - a perceiving and recognizing automaton. Technical Report 85-460-1, Cornell Aeronautical Laboratory, 1957.

E. Rosenfeld, P. Ravikumar, and A. Risteski. Domain-adjusted regression or: Erm may already learn features sufficient for out-of-distribution generalization. *arXiv preprint arXiv:2202.06856*, 2022.

S. Sagawa*, P. W. Koh*, T. B. Hashimoto, and P. Liang. Distributionally robust neural networks. In *International Conference on Learning Representations*, 2020.

W. Samek, G. Montavon, A. Vedaldi, L. K. Hansen, and K.-R. Muller. *Explainable AI: Interpreting, Explaining and Visualizing Deep Learning*. Springer Publishing Company, Incorporated, 1st edition, 2019. ISBN 3030289532.

V. Sanh, L. Debut, J. Chaumond, and T. Wolf. Distilbert, a distilled version of BERT: smaller, faster, cheaper and lighter. *arXiv preprint arXiv:1910.01108*, 2019.

H. Shah, K. Tamuly, A. Raghunathan, P. Jain, and P. Netrapalli. The pitfalls of simplicity bias in neural networks. In *Advances in Neural Information Processing Systems*, pages 9573–9585, 2020.

R. Shen, S. Bubeck, and S. Gunasekar. Data augmentation as feature manipulation. In *International Conference on Machine Learning*, pages 19773–19808, 2022.

Y. Shi, J. Seely, P. Torr, S. N, A. Hannun, N. Usunier, and G. Synnaeve. Gradient matching for domain generalization. In *International Conference on Learning Representations*, 2022.

R. Shwartz-Ziv and N. Tishby. Opening the black box of deep neural networks via information. *arXiv preprint arXiv:1703.00810*, 2017.

J. Taylor, B. Earnshaw, B. Mabey, M. Victors, and J. Yosinski. Rxrx1: An image set for cellular morphological variation across many experimental batches. In *International Conference on Learning Representations*, 2019.

D. Teney, Y. Lin, S. J. Oh, and E. Abbasnejad. ID and OOD performance are sometimes inversely correlated on real-world datasets. *arXiv preprint arXiv:2209.00613*, 2022.

V. Vapnik. Principles of risk minimization for learning theory. In *Advances in Neural Information Processing Systems*, pages 831–838, 1991.

Y. Wald, A. Feder, D. Greenfeld, and U. Shalit. On calibration and out-of-domain generalization. In *Advances in Neural Information Processing Systems*, pages 2215–2227, 2021.

Z. Wen and Y. Li. Toward understanding the feature learning process of self-supervised contrastive learning. In *International Conference on Machine Learning*, pages 11112–11122, 2021.

F. Wenzel, A. Dittadi, P. V. Gehler, C.-J. Simon-Gabriel, M. Horn, D. Zietlow, D. Kernert, C. Russell, T. Brox, B. Schiele, B. Schölkopf, and F. Locatello. Assaying out-of-distribution generalization in transfer learning. In *Advances in Neural Information Processing Systems*, 2022.

M. Wortsman, G. Ilharco, J. W. Kim, M. Li, S. Kornblith, R. Roelofs, R. G. Lopes, H. Hajishirzi, A. Farhadi, H. Namkoong, and L. Schmidt. Robust fine-tuning of zero-shot models. In *IEEE/CVF Conference on Computer Vision and Pattern Recognition*, pages 7949–7961, 2022.

H. Ye, J. Zou, and L. Zhang. Freeze then train: Towards provable representation learning under spurious correlations and feature noise. *arXiv preprint arXiv:2210.11075*, 2022.

J. Zhang and L. Bottou. Learning useful representations for shifting tasks and distributions. *arXiv preprint arXiv:2212.07346*, 2022.

J. Zhang, D. Lopez-Paz, and L. Bottou. Rich feature construction for the optimization-generalization dilemma. In *International Conference on Machine Learning*, pages 26397–26411, 2022.

D. Zou, Y. Cao, Y. Li, and Q. Gu. Understanding the generalization of adam in learning neural networks with proper regularization. *arXiv preprint arXiv:2108.11371*, 2021.

A. Limitations and Future Directions

As a pioneering work that studies feature learning of ERM and OOD objectives and their interactions in OOD generalization, our theoretical settings are limited to studying the influence of spurious and invariant correlation strengths on spurious and invariant feature learning, based on a two-layer CNN network. In fact, the feature learning of a network can be influenced by several other factors, such as the difficulty of learning a feature and the capacity of features that a model can learn (Hermann and Lampinen, 2020; Elhage et al., 2022). Future works can be built by extending our framework to consider the influence of a broad of factors on feature learning in OOD generalization.

Moreover, as there could exist cases where certain features should not be learned, it is also promising to explore how to prevent the feature learning of undesirable features during the early stages of OOD generalization and to further relieve the optimization dilemma in OOD generalization (Chen et al., 2022).

B. Related Work

On Feature Learning and Generalization. Understanding feature learning in deep networks is crucial to understanding their generalization (Rosenblatt, 1957; Shwartz-Ziv and Tishby, 2017; Brutzkus et al., 2018; Frei et al., 2021; Allen-Zhu and Li, 2020; Cao et al., 2022). Earlier attempts are mostly about empirical probing (Samek et al., 2019; Gupta et al., 2022; Hermann and Lampinen, 2020; Elhage et al., 2022). Hermann and Lampinen (2020); Elhage et al. (2022); Shah et al. (2020) find that the feature learning of a network can be influenced by several other factors, such as the difficulty of learning a feature and the capacity of features that a model can learn. Although our data model focuses on the correlation perspective, different correlation strengths in fact can simulate the difficulty or the simplicity of learning a feature.

Beyond the empirical probing, Allen-Zhu and Li (2020) proposed a new theoretical framework that characterizes the feature learning process of deep networks, which has been widely adopted to analyze behaviors of deep networks (Wen and Li, 2021; Zou et al., 2021; Cao et al., 2022) However, how the learned features from ID data can generalize to OOD data remains elusive. The only exceptions are (Shen et al., 2022) and (Kumar et al., 2022a). Kumar et al. (2022a) find fine-tuning can distort the pre-trained features while fine-tuning can be considered as a special case in our framework. Shen et al. (2022) focus on how data augmentation helps promote good but hard-to-learn features and improve OOD generalization. In contrast, we study the direct effects of ERM and OOD objectives to feature learning and provide a theoretical explanation to the phenomenon that ERM may have already learned good features (Rosenfeld et al., 2022; Izmailov et al., 2022).

On the correlation between ID and OOD performances. The debate about feature learning and generalization under distribution shifts also extends to the ID and OOD performance correlations along with training or fine-tuning neural nets across a variety of OOD generalization tasks. Andreassen et al. (2021); Miller et al. (2021); Wenzel et al. (2022) found that there often exists a linear dependency between ID and OOD performance under a wide range of models and distribution shifts. While Kumar et al. (2022a); Wortsman et al. (2022) found that fine-tuning pre-trained models often lead to an increased in-distribution but decreased OOD performance. Teney et al. (2022) observed cases where ID and OOD performance are inversely correlated. Chen et al. (2022); Naganuma et al. (2022) studied the ID and OOD performance trade-offs from the optimization perspective.

Our work provides theoretical explanations for different correlation behaviors of ID and OOD performance, as well as provides a solution for mitigating the trade-offs in optimization. Theorem 3.1 implies that, in cases where invariant features are more informative than spurious features, the higher ID performance indicates a better fit to invariant features, thus promising a higher OOD performance, aligned with observations in (Andreassen et al., 2021; Miller et al., 2021; Wenzel et al., 2022). While in cases where invariant features are less informative than spurious features, the higher ID performance implies a better fit to spurious features, thus bringing a lower OOD performance (Teney et al., 2022). The discussion also generalizes to fine-tuning pre-trained models, where ERM can lead to a better fit for spurious features and distort the previously learned invariant features (Kumar et al., 2022a; Wortsman et al., 2022).

Rich Feature Learning. Recently many OOD objectives have been proposed to regularize ERM such that the model can focus on learning invariant features (Arjovsky et al., 2019; Krueger et al., 2021; Pezeshki et al., 2021; Wald et al., 2021; Rame et al., 2021). However, due to the intrinsic conflicts of ERM and OOD objectives, it often requires exhaustive hyperparameter tuning of ERM pre-training epochs and regularization weights (Zhang et al., 2022; Chen et al., 2022). Especially, the final OOD performance has a large dependence on the number of pre-training epochs. To remedy the issue, Zhang et al. (2022) proposed Bonsai to construct rich feature representations with plentiful potentially useful features as network initialization. Although both Bonsai and FAT perform DRO on grouped subsets, Bonsai rely on multiple initializations of the whole network to capture diverse features from the subsets, and complicated ensembling of the features, which requires much more training epochs for the convergence. In contrast, FAT relieves the requirements by performing direct augmentation-retention on the grouped subsets, and thus obtains better performance. More crucially, although Bonsai and other rich feature learning algorithms such as weight averaging (Rame et al., 2022; Arpit et al., 2022; Zhang and Bottou, 2022) have gained impressive successes in mitigating the dilemma, explanations about the reliance on ERM pre-training and why rich feature learning mitigates the dilemma remain elusive. Our work provides novel theoretical explanations for the success of rich feature learning algorithms for OOD generalization. Complementary to the empirical observations made by existing works, our work provides the first theoretical explanation for the feature learning of ERM and OOD objectives for OOD generalization.

C. Preliminaries and Problem Definition

Notations. We use bold-faced letters for vectors and matrices otherwise for scalar. We use $\|\cdot\|_2$ to denote the Euclidean norm of a vector or the spectral norm of a matrix, while denoting $\|\cdot\|_F$ as the Frobenius norm of a matrix. $\mathbf{I}_d$ refers to the identity matrix with a dimension of $\mathbb{R}^{d\times d}$.

Our data model $\mathcal{D}=\{\mathbf{x}_i,y_i\}_{i=1}^n$ is adapted from (Allen-Zhu and Li, 2020) and further characterizes each data point $\mathbf{x}_i$ as invariant and spurious feature patches from the two-bit model (Kamath et al., 2021; Chen et al., 2022).

Definition C.1. $\mathcal{D}=\{\mathcal{D}_e\}_{e\in\mathcal{E}_{\text{all}}}$ is composed of multiple subsets $\mathcal{D}_e$ from different environments $e\in\mathcal{E}_{\text{all}}$, where each $\mathcal{D}_e=\{(\mathbf{x}_i^e,y_i^e)\}_{i=1}^{n_e}$ is composed of i.i.d. samples $(\mathbf{x}_i^e,y_i^e)\sim\mathbb{P}^e$. Each data $(\mathbf{x}^e,y^e)\in\mathcal{D}_e$ with $\mathbf{x}^e\in\mathbb{R}^{2d}$ and $y^e\in\{-1,1\}$ is generated as follows:

(a) Sample $y^e\in\{-1,1\}$ uniformly;

(b) Given y^e, each input $\mathbf{x}^e=[\mathbf{x}_1^e,\mathbf{x}_2^e]$ contains a feature patch $\mathbf{x}_1$ and a noise patch $\mathbf{x}_2$, that are sampled as:

$$\mathbf{x}_1=y\cdot\text{Rad}(\alpha)\cdot\mathbf{v}_1+y\cdot\text{Rad}(\beta)\cdot\mathbf{v}_2\quad \mathbf{x}_2=\boldsymbol{\xi}$$

where $\text{Rad}(\delta)$ is a random variable taking value -1 with probability δ and $+1$ with probability $1-\delta$, $\mathbf{v}_1=[1,0,\ldots 0]^\top$ and $\mathbf{v}_2=[0,1,0,\ldots 0]^\top$.

(c) A noise vector $\boldsymbol{\xi}$ is generated from the Gaussian distribution $\mathcal{N}(\mathbf{0},\sigma_p^2\cdot(\mathbf{I}_d-\mathbf{v}_1\mathbf{v}_1^\top-\mathbf{v}_2\mathbf{v}_2^\top))$

Definition 2.1 is inspired by the structure of image data in image classification with CNN (Allen-Zhu and Li, 2020), where the inputs consist of different patches, some of the patches consist of features that are related to the class label of the image, and the others are noises that are irrelevant to the label. In particular, $\mathbf{v}_1$ and $\mathbf{v}_2$ are feature vectors that simulate the invariant and spurious features, respectively. Although our data model focuses on two feature vectors, the discussion and results can be further generalized to multiple invariant and spurious features with fine-grained characteristics (Shen et al., 2022). Following previous works (Cao et al., 2022), we assume that the noise patch is generated from the Gaussian distribution such that the noise vector is orthogonal to the signal vector $\mathbf{v}$. Each environment is denoted as $\mathcal{E}_\alpha=\{(\alpha,\beta_e):0<\beta_e<1\}$, where $\mathbf{v}_1$ is the invariant feature as α is fixed while $\mathbf{v}_2$ is the spurious feature as β_e varies across e.

CNN model. We consider training a two-layer convolutional neural network with a hidden layer width of m. The filters are applied to $\mathbf{x}_1$, $\mathbf{x}_2$, respectively,[3] and the second layer parameters of the network are fixed as $\frac{1}{m}$ and $-\frac{1}{m}$, respectively. Then the network can be written as $f(\mathbf{W},\mathbf{x})=F_{+1}(\mathbf{W}_{+1},\mathbf{x})-F_{-1}(\mathbf{W}_{-1},\mathbf{x})$, where $F_{+1}(\mathbf{W}_{+1},\mathbf{x})$ and $F_{-1}(\mathbf{W}_{-1},\mathbf{x})$ are defined as follows:

$$F_j(\mathbf{W}_j,\mathbf{x})=\frac{1}{m}\sum_{r=1}^{m}\left[\sigma(\mathbf{w}_{j,r}^\top\mathbf{x}_1)+\sigma(\mathbf{w}_{j,r}^\top\mathbf{x}_2)\right], \tag{5}$$

where $\sigma(x)$ is the activation function. We assume that all network weights are initialized as $\mathcal{N}(0,\sigma_0^2)$. In this work, we focus on linear activation $\sigma(x)=x$ since it is sufficient to observe the desired feature learning behaviors of ERM and OOD objectives (i.e., the reliance to ERM pre-training).[4] Nevertheless, our framework can also be extended to non-linear activation functions, such as q-ReLU (Zou et al., 2021; Cao et al., 2022).

[3]When the environment e is not explicitly considered, we will omit it for clarity.

[4]It is also partially due to the complexity of IRMv1 dynamics, though to the best of our knowledge, we are the first to directly study the IRMv1 dynamics.

ERM objective. We train the CNN model by minimizing the empirical cross-entropy loss function:

$$L_S(\mathbf{W}) = \sum_{e \in \mathcal{E}_{\text{tr}}} \frac{1}{n_e} \sum_{i=1}^{n_e} \ell(y_i^e \cdot f(\mathbf{W}, \mathbf{x}_i^e)), \tag{6}$$

where $\ell(z) = \log(1+\exp(-z))$ and $\{\mathcal{D}_e\}_{e\in\mathcal{E}_{\text{tr}}} = \{\{\mathbf{x}_i^e, y_i^e\}_{i=1}^{n_e}\}_{e\in\mathcal{E}_{\text{tr}}}$ is the trainset with $\sum_{e\in\mathcal{E}_{\text{tr}}} n_e = n$.

OOD objective. The goal of OOD generalization is, given the data from training environments $\{\mathcal{D}_e\}_{e\in\mathcal{E}_{\text{tr}}}$, to find a predictor $f : \mathcal{X} \to \mathcal{Y}$ that generalizes well to all (unseen) environments, or minimizes $\max_{e\in\mathcal{E}_{\text{all}}} L_e(f)$, where L_e is the empirical risk under environment e. The predictor $f = w \circ \varphi$ is usually composed of a featurizer $\varphi : \mathcal{X} \to \mathcal{Z}$ that learns to extract useful features, and a classifier $w : \mathcal{Z} \to \mathcal{Y}$ that makes predictions from the extracted features.

Since we are interested in cases where the OOD objective succeeds in learning the invariant features. In the discussion below, without loss of generality, we study one of the most widely discussed OOD objective, IRMv1 objective, from IRM framework(Arjovsky et al., 2019), and the data model where IRMv1 succeeds. Specifically, the IRM framework approaches OOD generalization by finding an invariant representation φ, such that there exists a classifier acting on φ that is simultaneously optimal in $\mathcal{E}_{\text{tr}}$. Hence, IRM leads to a challenging bi-level optimization problem as

$$\min_{w,\varphi} \sum_{e\in\mathcal{E}_{\text{tr}}} L_e(w\circ\varphi), \text{s.t. } w \in \operatorname*{arg\,min}_{\bar{w}:\mathcal{Z}\to\mathcal{Y}} L_e(\bar{w}\circ\varphi),\ \forall e \in \mathcal{E}_{\text{tr}}. \tag{7}$$

Due to the optimization difficulty of Eq. (7), Arjovsky et al. (2019) relax Eq. (7) into IRMv1 as follows:

$$\min_{\varphi} \sum_{e\in\mathcal{E}_{\text{tr}}} L_e(\varphi) + \lambda |\nabla_{w|w=1} L_e(w\cdot\varphi)|^2. \tag{8}$$

Given the convolutional neural network (Eq. 5) and logistic loss (Eq. 6), IRMv1 can be written as

$$L_{\text{IRMv1}}(\mathbf{W}) = \sum_{e\in\mathcal{E}_{\text{tr}}} \frac{1}{n_e} \sum_{i=1}^{n_e} \ell\left(y_i^e \cdot f(\mathbf{W}, \mathbf{x}_i^e)\right) + \sum_{e\in\mathcal{E}_{\text{tr}}} \frac{\lambda}{n_e^2} \left(\sum_{i=1}^{n_e} \ell_i' \cdot y_i^e \cdot f(\mathbf{W}, \mathbf{x}_i^e) \right)^2, \tag{9}$$

where ${\ell'}_i^e = \ell'(y_i^e \cdot f(\mathbf{W}, \mathbf{x}_i^e)) = -\frac{\exp(-y_i^e\cdot f(\mathbf{W},\mathbf{x}_i^e))}{1+\exp(-y_i^e\cdot f(\mathbf{W},\mathbf{x}_i^e))}$. Following (Arjovsky et al., 2019), we define the featurizer φ as the whole CNN model and the classifier w as the scalar 1. Due to the complexity of IRMv1, in the analysis below, we introduce C^e_{IRMv1} for the ease of expressions. Specifically, we define C^e_{IRMv1} as

$$C^e_{\text{IRMv1}} \triangleq \frac{1}{n_e} \sum_{i=1}^{n_e} \ell'\left(y_i^e \hat{y}_i^e\right) \cdot y_i^e \hat{y}_i^e,$$

where $\hat{y}_i^e \triangleq f(\mathbf{W}, \mathbf{x}_i^e)$ is the logit of sample $\mathbf{x}_i$ from environment e. The convergence of C_{IRMv1} indicates the convergence of IRMv1 penalty. The following lemma will be useful in our analysis.

Lemma C.2. *(Cao et al. (2022)) Let $\mathbf{w}_{j,r}(t)$[5] for $j \in \{+1,-1\}$ and $r \in \{1,2,\dots,m\}$ be the convolution filters of the CNN at t-th iteration of gradient descent. Then there exists unique coefficients $\gamma_{j,r,1}(t), \gamma_{j,r,2}(t) \geq 0$ and $\rho_{j,r,i}(t)$ such that,*

$$\mathbf{w}_{j,r}(t) = \mathbf{w}_{j,r}(0) + j\cdot\gamma_{j,r,1}(t)\cdot\mathbf{v}_1 + j\cdot\gamma_{j,r,2}(t)\cdot\mathbf{v}_2 + \sum_{i=1}^{n} \rho_{j,r,i}(t)\cdot\|\boldsymbol{\xi}_i\|_2^{-2}\cdot\boldsymbol{\xi}_i. \tag{10}$$

We refer Eq. (10) as the *signal-noise decomposition* of $\mathbf{w}_{j,r}(t)$ (Cao et al., 2022). We add normalization factor $\|\boldsymbol{\xi}_i\|_2^{-2}$ in the definition so that $\rho_{j,r}^{(t)} \approx \langle \mathbf{w}_{j,r}^{(t)}, \boldsymbol{\xi}_i\rangle$. Note that $\|\mathbf{v}_1\|_2 = \|\mathbf{v}_2\|_2 = 1$, the corresponding normalization factors are thus neglected. Furthermore, $\gamma_{j,r,1} \approx \langle \mathbf{w}_{j,r}, \mathbf{v}_1\rangle$ and $\gamma_{j,r,2} \approx \langle \mathbf{w}_{j,r}, \mathbf{v}_2\rangle$ respectively denote the degrees of invariant and spurious feature learning. For ease of understanding, in the discussion below, we will denote $\gamma_{j,r,1}$ and $\gamma_{j,r,2}$ as $\gamma_{j,r}^{inv}$ and $\gamma_{j,r}^{spu}$, respectively.

[5] We use $\mathbf{w}_{j,r}(t)$, $\mathbf{w}_{j,r}^{(t)}$ and $\mathbf{w}_{j,r}^{t}$ interchangeably.

D. Proofs for theoretical results

Notations. We use bold-faced letters for vectors and matrices otherwise for scalar. We use $\|\cdot\|_2$ to denote the Euclidean norm of a vector or the spectral norm of a matrix, while denoting $\|\cdot\|_F$ as the Frobenius norm of a matrix. For a neural network, we denote $\sigma(x)$ as the activation function. Let $\mathbf{I}_d$ be the identity matrix with a dimension of $\mathbb{R}^{d\times d}$. We denote $[n]=\{1,2,\ldots,n\}$.

D.1. Implementation details of the synthetic CNN experiments

The logit $\hat{y}_i^e$ (which is a function of $\mathbf{W}$) of sample i in the environment e can be explicitly written as

$$\hat{y}_i^e = f(\mathbf{W},\mathbf{x}_i^e) = F_{+1}(\mathbf{W}_{+1},\mathbf{x}_i^e) - F_{-1}(\mathbf{W}_{-1},\mathbf{x}_i^e) = \sum_{j\in\{\pm1\}} \frac{j}{m}\sum_{r=1}^{m}\left[\mathbf{w}_{j,r}^\top(\mathbf{x}_{i,1}^e+\mathbf{x}_{i,2}^e)\right],$$

where $\mathbf{W}\triangleq\{\mathbf{W}_{+1},\mathbf{W}_{-1}\}$ and $\mathbf{W}_j \triangleq \begin{bmatrix}\mathbf{w}_{j,1}^\top\\ \vdots \\ \mathbf{w}_{j,m}^\top\end{bmatrix}$ for $j\in\{\pm1\}$. We initialized all the network weights as $\mathcal{N}(0,\sigma_0^2)$ and we set $\sigma_0=0.01$.

The test dataset $(\mathbf{x},y)$ is generated through

$$\mathbf{x}_{i,1} = y_i\cdot\mathbf{v}_1 + y_i\cdot\mathrm{Rad}(1-\beta_e)\cdot\mathbf{v}_2, \qquad \mathbf{x}_{i,2}=\boldsymbol{\xi},$$

where half of the dataset uses $\mathrm{Rad}(1-\beta_1)$ and the other half uses $\mathrm{Rad}(1-\beta_2)$. Here $\boldsymbol{\xi}\sim\mathcal{N}(0,\sigma_p^2\cdot(\mathbf{I}_d-\mathbf{v}_1\mathbf{v}_1^\top-\mathbf{v}_2\mathbf{v}_2^\top))$ and we chose $\sigma_p=0.01$.

From the definition of IRMv1, we take derivative wrt the scalar 1 of the logit $1\cdot\hat{y}_i^e$. Thus, for environment e, the penalty is

$$\left(\frac{1}{n_e}\sum_{i=1}^{n_e}\nabla_{w|w=1}\ell\big(y_i^e(w\cdot\hat{y}_i^e)\big)\right)^2 = \left(\frac{1}{n_e}\sum_{i=1}^{n_e}\ell'\big(y_i^e\hat{y}_i^e\big)\cdot y_i^e\hat{y}_i^e\right)^2.$$

Then, the IRMv1 objective is (we set $n_1=n_2=2500$ in the simulation)

$$L_{\text{IRMv1}}(\mathbf{W}) = \sum_{e\in\mathcal{E}_{tr}}\frac{1}{n_e}\sum_{i=1}^{n_e}\ell\big(y_i^e\hat{y}_i^e\big) + \lambda\sum_{e\in\mathcal{E}_{tr}}\left(\frac{1}{n_e}\sum_{i=1}^{n_e}\ell'\big(y_i^e\hat{y}_i^e\big)\cdot y_i^e\hat{y}_i^e\right)^2.$$

We used constant stepsize GD to minimize $L_{\text{IRMv1}}(\mathbf{W})$, and we chose $\lambda=10^8$ (heavy regularization setup).

Let $C_{\text{IRMv1}}^e \triangleq \frac{1}{n_e}\sum_{i=1}^{n_e}\ell'\big(y_i^e\hat{y}_i^e\big)\cdot y_i^e\hat{y}_i^e$. The gradient of $L_{\text{IRMv1}}(\mathbf{W})$ with respect to each $\mathbf{w}_{j,r}$ can be explicitly written as

$$\begin{aligned}
\nabla_{\mathbf{w}_{j,r}}L_{\text{IRMv1}}(\mathbf{W}) =& \sum_{e\in\mathcal{E}_{tr}}\frac{1}{n_e}\sum_{i=1}^{n_e}\ell'\big(y_i^e\hat{y}_i^e\big)\cdot y_i^e\cdot\frac{j}{m}(\mathbf{x}_{i,1}^e+\mathbf{x}_{i,2}^e)\\
&+2\lambda\sum_{e\in\mathcal{E}_{tr}}\frac{C_{\text{IRMv1}}^e}{n_e}\sum_{i=1}^{n_e}\Big(\ell''\big(y_i^e\hat{y}_i^e\big)\cdot\hat{y}_i^e\cdot\frac{j}{m}(\mathbf{x}_{i,1}^e+\mathbf{x}_{i,2}^e)+\ell'\big(y_i^e\hat{y}_i^e\big)\cdot y_i^e\cdot\frac{j}{m}(\mathbf{x}_{i,1}^e+\mathbf{x}_{i,2}^e)\Big)\\
=& \sum_{e\in\mathcal{E}_{tr}}\frac{j}{n_e m}\sum_{i=1}^{n_e}\ell'\big(y_i^e\hat{y}_i^e\big)\cdot y_i^e\cdot(\mathbf{x}_{i,1}^e+\mathbf{x}_{i,2}^e) + 2\lambda\sum_{e\in\mathcal{E}_{tr}}\frac{jC_{\text{IRMv1}}^e}{n_e m}\sum_{i=1}^{n_e}\ell''\big(y_i^e\hat{y}_i^e\big)\cdot\hat{y}_i^e\cdot(\mathbf{x}_{i,1}^e+\mathbf{x}_{i,2}^e)\\
&+2\lambda\sum_{e\in\mathcal{E}_{tr}}\frac{jC_{\text{IRMv1}}^e}{n_e m}\sum_{i=1}^{n_e}\ell'\big(y_i^e\hat{y}_i^e\big)\cdot y_i^e\cdot(\mathbf{x}_{i,1}^e+\mathbf{x}_{i,2}^e)\\
=& \sum_{e\in\mathcal{E}_{tr}}\frac{j(1+2\lambda C_{\text{IRMv1}}^e)}{n_e m}\sum_{i=1}^{n_e}\ell'\big(y_i^e\hat{y}_i^e\big)\cdot y_i^e\cdot(\mathbf{x}_{i,1}^e+\mathbf{x}_{i,2}^e)\\
&+2\lambda\sum_{e\in\mathcal{E}_{tr}}\frac{jC_{\text{IRMv1}}^e}{n_e m}\sum_{i=1}^{n_e}\ell''\big(y_i^e\hat{y}_i^e\big)\cdot\hat{y}_i^e\cdot(\mathbf{x}_{i,1}^e+\mathbf{x}_{i,2}^e).
\end{aligned}$$

Observe that C^e_{IRMv1} is in fact the scalar gradient $C^e_{\text{IRMv1}} = \nabla_{w|w=1} L^e_{\text{ERM}}(\mathbf{W})$ that we want to force zero, whose effect can be understood as a dynamic re-weighting of the ERM gradient. Due to its importance in the analysis and interpretation of IRMv1, we tracked C^e_{IRMv1} in our simulations.

The invariant and spurious feature learning terms that we tracked are the mean of $\langle \mathbf{w}_{j,r}, j\mathbf{v}_1\rangle$ and $\langle \mathbf{w}_{j,r}, j\mathbf{v}_2\rangle$ for $j \in \{\pm 1\}, r \in [m]$, respectively.

D.2. Proof for Theorem 3.1

Theorem D.1 (Formal statement of Theorem 3.1)**.** *For $\rho > 0$, denote $\underline{n} \triangleq \min_{e\in\mathcal{E}_{tr}} n_e$, $n \triangleq \sum_{e\in\mathcal{E}_{tr}} n_e$, $\epsilon_C \triangleq \sqrt{\frac{2\log(16/\rho)}{\underline{n}}}$ and $\delta \triangleq \exp\{O(\underline{n}^{-1})\} - 1$. Define the feature learning terms $\Lambda^t_{j,r} \triangleq \langle \mathbf{w}^t_{j,r}, j\mathbf{v}_1\rangle$ and $\Gamma^t_{j,r} \triangleq \langle \mathbf{w}^t_{j,r}, j\mathbf{v}_2\rangle$ for $j \in \{\pm 1\}, r \in [m]$. Suppose we run T iterations of GD for the ERM objective. With sufficiently large $\underline{n}$, assuming that*

$$
\begin{aligned}
&\alpha, \beta_1, \beta_2 < \frac{1 - \epsilon_C - \delta(\frac{1}{4} + \frac{\epsilon_C}{2})}{2} \quad (\alpha, \beta_1, \beta_2 \text{ are sufficiently smaller than } \frac{1}{2}),\\
&\alpha > \frac{\beta_1 + \beta_2}{2} + \epsilon_C + \frac{\delta(1+\epsilon_C)}{2} \quad (\alpha \text{ is sufficiently larger than } \frac{\beta_1+\beta_2}{2}),
\end{aligned}
$$

and choosing

$$
\begin{aligned}
\sigma_0^2 &= O\left(\underline{n}^{-2}\log^{-1}(m/\rho)\right),\\
\sigma_p^2 &= O\left(\min\left\{d^{-1/2}\log^{-1/2}(nm/\rho), T^{-1}\eta^{-1}m\left(d + n\sqrt{d\log(n^2/\rho)}\right)^{-1}\right\}\right),
\end{aligned}
$$

there exists a constant η, such that for any $j \in \{\pm 1\}, r \in [m]$, with probability at least $1 - 2\rho$, $\Lambda^t_{j,r}$ and $\Gamma^t_{j,r}$ are converging and the increment of the spurious feature $\Gamma^{t+1}_{j,r} - \Gamma^t_{j,r}$ is larger than that of the invariant feature $\Lambda^{t+1}_{j,r} - \Lambda^t_{j,r}$ at any iteration $t \in \{0, \ldots, T-1\}$.

Proof of Theorem D.1. We begin with checking the feature learning terms in the ERM stage using constant stepsize GD: $\mathbf{W}^{t+1} = \mathbf{W}^t - \eta \cdot \nabla_{\mathbf{W}} L_{\text{IRMv1}}(\mathbf{W}^t)$. Note that the update rule for each $\mathbf{w}_{j,r}, \forall j \in \{+1, -1\}, r \in [m]$ can be written as

$$
\begin{aligned}
\mathbf{w}^{t+1}_{j,r} &= \mathbf{w}^t_{j,r} - \frac{j\eta}{m}\sum_{e\in\mathcal{E}_{tr}}\frac{1}{n_e}\sum_{i=1}^{n_e}\ell'\left(y^e_i\hat{y}^e_i\right)\cdot y^e_i \cdot (\mathbf{x}^e_{i,1} + \mathbf{x}^e_{i,2})\\
&= \mathbf{w}^t_{j,r} - \frac{j\eta}{m}\sum_{e\in\mathcal{E}_{tr}}\frac{1}{n_e}\sum_{i=1}^{n_e}\ell'\left(y^e_i\hat{y}^e_i\right)\cdot (\text{Rad}(\alpha)_i \cdot \mathbf{v}_1 + \text{Rad}(\beta_e)_i \cdot \mathbf{v}_2 + y^e_i\boldsymbol{\xi}^e_i).
\end{aligned}
$$

Define the quantities of interest (the feature learning terms): $\Lambda^t_{j,r} \triangleq \langle \mathbf{w}^t_{j,r}, j\mathbf{v}_1\rangle, \Gamma^t_{j,r} \triangleq \langle \mathbf{w}^t_{j,r}, j\mathbf{v}_2\rangle, \Xi^{t,e}_{j,r,i} \triangleq \langle \mathbf{w}^t_{j,r}, j\boldsymbol{\xi}^e_i\rangle$. From our data generating procedure (Definition 2.1), we know that the first two coordinates of $\boldsymbol{\xi}^e_i$ are zero. Thus, we can write down the update rule for each feature learning term as follows.

$$
\begin{aligned}
\Lambda^{t+1}_{j,r} &= \Lambda^t_{j,r} - \frac{\eta}{m}\sum_{e\in\mathcal{E}_{tr}}\frac{1}{n_e}\sum_{i=1}^{n_e}\ell'\left(y^e_i\hat{y}^e_i\right)\cdot \text{Rad}(\alpha)_i,\\
\Gamma^{t+1}_{j,r} &= \Gamma^t_{j,r} - \frac{\eta}{m}\sum_{e\in\mathcal{E}_{tr}}\frac{1}{n_e}\sum_{i=1}^{n_e}\ell'\left(y^e_i\hat{y}^e_i\right)\cdot \text{Rad}(\beta_e)_i,\\
\Xi^{t+1,e'}_{j,r,i'} &= \Xi^{t,e'}_{j,r,i'} - \frac{\eta}{m}\sum_{e\in\mathcal{E}_{tr}}\frac{1}{n_e}\sum_{i=1}^{n_e}\ell'\left(y^e_i\hat{y}^e_i\right)\cdot y^e_i\cdot\langle\boldsymbol{\xi}^e_i, \boldsymbol{\xi}^{e'}_{i'}\rangle.
\end{aligned}
$$

More explicitly, we can write

$$\Lambda_{j,r}^{t+1} = \Lambda_{j,r}^{t} + \frac{\eta}{m} \sum_{e\in\mathcal{E}_{tr}} \frac{1}{n_e} \sum_{i=1}^{n_e} \frac{\mathrm{Rad}(\alpha)_i}{1+\exp\{y_i^e \hat{y}_i^e\}}, \tag{11}$$

$$\Gamma_{j,r}^{t+1} = \Gamma_{j,r}^{t} + \frac{\eta}{m} \sum_{e\in\mathcal{E}_{tr}} \frac{1}{n_e} \sum_{i=1}^{n_e} \frac{\mathrm{Rad}(\beta_e)_i}{1+\exp\{y_i^e \hat{y}_i^e\}}, \tag{12}$$

$$\Xi_{j,r,i'}^{t+1,e'} = \Xi_{j,r,i'}^{t,e'} + \frac{\eta}{m} \sum_{e\in\mathcal{E}_{tr}} \frac{1}{n_e} \sum_{i=1}^{n_e} \frac{y_i^e \cdot \langle \boldsymbol{\xi}_i^e, \boldsymbol{\xi}_{i'}^{e'} \rangle}{1+\exp\{y_i^e \hat{y}_i^e\}}. \tag{13}$$

Notice that the updates (11), (12) for $\Lambda_{j,r}, \Gamma_{j,r}$ are independent of j, r. Denoting

$$\Delta_\Lambda^t \triangleq \frac{1}{m} \sum_{e\in\mathcal{E}_{tr}} \frac{1}{n_e} \sum_{i=1}^{n_e} \frac{\mathrm{Rad}(\alpha)_i}{1+\exp\{y_i^e \hat{y}_i^e\}},$$

$$\Delta_\Gamma^t \triangleq \frac{1}{m} \sum_{e\in\mathcal{E}_{tr}} \frac{1}{n_e} \sum_{i=1}^{n_e} \frac{\mathrm{Rad}(\beta_e)_i}{1+\exp\{y_i^e \hat{y}_i^e\}},$$

we can conclude that for any $j \in \{+1, -1\}, r \in [m]$,

$$\begin{aligned} \Lambda_{j,r}^{t+1} &= \Lambda_{j,r}^{t} + \eta \cdot \Delta_\Lambda^t = \eta \cdot \sum_{k=0}^{t} \Delta_\Lambda^k + \Lambda_{j,r}^0, \\ \Gamma_{j,r}^{t+1} &= \Gamma_{j,r}^{t} + \eta \cdot \Delta_\Gamma^t = \eta \cdot \sum_{k=0}^{t} \Delta_\Gamma^k + \Gamma_{j,r}^0. \end{aligned} \tag{14}$$

Then, we write the logit $\hat{y}_i^e$ as

$$\begin{aligned} \hat{y}_i^e = &\sum_{j\in\{\pm1\}} \frac{j}{m} \sum_{r=1}^{m} \left[\langle \mathbf{w}_{j,r}^t, y_i^e \cdot \mathrm{Rad}(\alpha)_i \cdot \mathbf{v}_1 + y_i^e \cdot \mathrm{Rad}(\beta_e)_i \cdot \mathbf{v}_2 + \mathbf{x}_{i,2}^e \rangle\right] \\ = &\sum_{j\in\{\pm1\}} \frac{j}{m} \sum_{r=1}^{m} \left[j y_i^e \cdot \mathrm{Rad}(\alpha)_i \cdot \Lambda_{j,r}^t + j y_i^e \cdot \mathrm{Rad}(\beta_e)_i \cdot \Gamma_{j,r}^t + j \cdot \Xi_{j,r,i}^{t,e}\right] \\ = &\sum_{j\in\{\pm1\}} \frac{1}{m} \sum_{r=1}^{m} \left[y_i^e \cdot \mathrm{Rad}(\alpha)_i \cdot \Lambda_{j,r}^t + y_i^e \cdot \mathrm{Rad}(\beta_e)_i \cdot \Gamma_{j,r}^t + \Xi_{j,r,i}^{t,e}\right] \\ = &\, y_i^e \cdot \mathrm{Rad}(\alpha)_i \cdot \sum_{j\in\{\pm1\}} \sum_{r=1}^{m} \frac{\Lambda_{j,r}^t}{m} + y_i^e \cdot \mathrm{Rad}(\beta_e)_i \cdot \sum_{j\in\{\pm1\}} \sum_{r=1}^{m} \frac{\Gamma_{j,r}^t}{m} + \sum_{j\in\{\pm1\}} \sum_{r=1}^{m} \frac{\Xi_{j,r,i}^{t,e}}{m} \\ = &\, y_i^e \cdot \mathrm{Rad}(\alpha)_i \cdot 2\eta \cdot \sum_{k=0}^{t-1} \Delta_\Lambda^k + y_i^e \cdot \mathrm{Rad}(\beta_e)_i \cdot 2\eta \cdot \sum_{k=0}^{t-1} \Delta_\Gamma^k \\ &+ y_i^e \cdot \mathrm{Rad}(\alpha)_i \cdot \sum_{j\in\{\pm1\}} \sum_{r=1}^{m} \frac{\Lambda_{j,r}^0}{m} + y_i^e \cdot \mathrm{Rad}(\beta_e)_i \cdot \sum_{j\in\{\pm1\}} \sum_{r=1}^{m} \frac{\Gamma_{j,r}^0}{m} + \sum_{j\in\{\pm1\}} \sum_{r=1}^{m} \frac{\Xi_{j,r,i}^{t,e}}{m}. \end{aligned}$$

Denoting $\mathbb{Q}_i^e \triangleq \mathrm{Rad}(\alpha)_i \sum_{j\in\{\pm1\}} \sum_{r=1}^{m} \frac{\Lambda_{j,r}^0}{m} + \mathrm{Rad}(\beta_e)_i \sum_{j\in\{\pm1\}} \sum_{r=1}^{m} \frac{\Gamma_{j,r}^0}{m} + y_i^e \cdot \sum_{j\in\{\pm1\}} \sum_{r=1}^{m} \frac{\Xi_{j,r,i}^{t,e}}{m}$, we have

$$\hat{y}_i^e = y_i^e \cdot \left(\mathrm{Rad}(\alpha)_i \cdot 2\eta \cdot \sum_{k=0}^{t-1} \Delta_\Lambda^k + \mathrm{Rad}(\beta_e)_i \cdot 2\eta \cdot \sum_{k=0}^{t-1} \Delta_\Gamma^k + \mathbb{Q}_i^e\right),$$

We need the following concentration lemma to control the scale of $\mathbb{Q}_i^e$, whose proof is given in Appendix D.2.1.

Lemma D.2. *Denote* $\underline{n} \triangleq \min_{e\in\mathcal{E}_{tr}} n_e, n \triangleq \sum_{e\in\mathcal{E}_{tr}} n_e$. *For* $\rho > 0$, *if*

$$\sigma_0^2 = O\left(\underline{n}^{-2}\log^{-1}(m/\rho)\right),$$
$$\sigma_p^2 = O\left(\min\left\{d^{-1/2}\log^{-1/2}(nm/\rho), T^{-1}\eta^{-1}m\left(d + n\sqrt{d\log(n^2/\rho)}\right)^{-1}\right\}\right),$$

then with probability at least $1-\rho$, *for any* $e \in \mathcal{E}_{tr}, i \in [n_e]$, *it holds that* $|\mathbb{Q}_i^e| = O(\underline{n}^{-1})$.

Then Δ_Λ^t and Δ_Γ^t can be explicitly written as

$$\Delta_\Lambda^t = \sum_{e\in\mathcal{E}_{tr}} \frac{1}{n_e m}\sum_{i=1}^{n_e} \frac{\mathrm{Rad}(\alpha)_i}{1+\exp\left\{\mathrm{Rad}(\alpha)_i\cdot 2\eta\cdot\sum_{k=0}^{t-1}\Delta_\Lambda^k\right\}\cdot\exp\left\{\mathrm{Rad}(\beta_e)_i\cdot 2\eta\cdot\sum_{k=0}^{t-1}\Delta_\Gamma^k\right\}\cdot\exp\left\{\mathbb{Q}_i^e\right\}},$$
$$\Delta_\Gamma^t = \sum_{e\in\mathcal{E}_{tr}} \frac{1}{n_e m}\sum_{i=1}^{n_e} \frac{\mathrm{Rad}(\beta_e)_i}{1+\exp\left\{\mathrm{Rad}(\alpha)_i\cdot 2\eta\cdot\sum_{k=0}^{t-1}\Delta_\Lambda^k\right\}\cdot\exp\left\{\mathrm{Rad}(\beta_e)_i\cdot 2\eta\cdot\sum_{k=0}^{t-1}\Delta_\Gamma^k\right\}\cdot\exp\left\{\mathbb{Q}_i^e\right\}}.$$

We are going to analyze the convergences of two sequences $\{\Delta_\Gamma^t + \Delta_\Lambda^t\}$ and $\{\Delta_\Gamma^t - \Delta_\Lambda^t\}$. Notice that

$$\Delta_\Gamma^t + \Delta_\Lambda^t = \sum_{e\in\mathcal{E}_{tr}} \frac{1}{n_e m}\sum_{i=1}^{n_e} \frac{\mathrm{Rad}(\beta_e)_i + \mathrm{Rad}(\alpha)_i}{1+\exp\left\{\mathrm{Rad}(\alpha)_i\cdot 2\eta\cdot\sum_{k=0}^{t-1}\Delta_\Lambda^k\right\}\cdot\exp\left\{\mathrm{Rad}(\beta_e)_i\cdot 2\eta\cdot\sum_{k=0}^{t-1}\Delta_\Gamma^k\right\}\cdot\exp\left\{\mathbb{Q}_i^e\right\}},$$
$$\Delta_\Gamma^t - \Delta_\Lambda^t = \sum_{e\in\mathcal{E}_{tr}} \frac{1}{n_e m}\sum_{i=1}^{n_e} \frac{\mathrm{Rad}(\beta_e)_i - \mathrm{Rad}(\alpha)_i}{1+\exp\left\{\mathrm{Rad}(\alpha)_i\cdot 2\eta\cdot\sum_{k=0}^{t-1}\Delta_\Lambda^k\right\}\cdot\exp\left\{\mathrm{Rad}(\beta_e)_i\cdot 2\eta\cdot\sum_{k=0}^{t-1}\Delta_\Gamma^k\right\}\cdot\exp\left\{\mathbb{Q}_i^e\right\}}.$$

We can further write these two terms as

$$\begin{aligned}
\Delta_\Gamma^t + \Delta_\Lambda^t = &\sum_{e\in\mathcal{E}_{tr}} \frac{2}{n_e m} \sum_{\substack{i\in[n_e]\\ \mathrm{Rad}(\beta_e)_i=+1\\ \mathrm{Rad}(\alpha)_i=+1}} \frac{1}{1+\exp\left\{2\eta\cdot\sum_{k=0}^{t-1}(\Delta_\Gamma^k+\Delta_\Lambda^k)\right\}\cdot\exp\left\{\mathbb{Q}_i^e\right\}}\\
&- \sum_{e\in\mathcal{E}_{tr}} \frac{2}{n_e m} \sum_{\substack{i\in[n_e]\\ \mathrm{Rad}(\beta_e)_i=-1\\ \mathrm{Rad}(\alpha)_i=-1}} \frac{1}{1+\exp\left\{-2\eta\cdot\sum_{k=0}^{t-1}(\Delta_\Gamma^k+\Delta_\Lambda^k)\right\}\cdot\exp\left\{\mathbb{Q}_i^e\right\}},\\
\Delta_\Gamma^t - \Delta_\Lambda^t = &\sum_{e\in\mathcal{E}_{tr}} \frac{2}{n_e m} \sum_{\substack{i\in[n_e]\\ \mathrm{Rad}(\beta_e)_i=+1\\ \mathrm{Rad}(\alpha)_i=-1}} \frac{1}{1+\exp\left\{2\eta\cdot\sum_{k=0}^{t-1}(\Delta_\Gamma^k-\Delta_\Lambda^k)\right\}\cdot\exp\left\{\mathbb{Q}_i^e\right\}}\\
&- \sum_{e\in\mathcal{E}_{tr}} \frac{2}{n_e m} \sum_{\substack{i\in[n_e]\\ \mathrm{Rad}(\beta_e)_i=-1\\ \mathrm{Rad}(\alpha)_i=+1}} \frac{1}{1+\exp\left\{-2\eta\cdot\sum_{k=0}^{t-1}(\Delta_\Gamma^k-\Delta_\Lambda^k)\right\}\cdot\exp\left\{\mathbb{Q}_i^e\right\}}.
\end{aligned}$$

According to Lemma D.2, for all $e \in \mathcal{E}_{tr}, i \in [n_e], \rho > 0$, letting $\delta \triangleq \exp\{O(\underline{n}^{-1})\} - 1$, we have $1+\delta \geq \exp\left\{\mathbb{Q}_i^e\right\} \geq (1+\delta)^{-1}$ with probability at least $1-\rho$. Let $C_{j\ell}^e \triangleq |\{i \mid \mathrm{Rad}(\alpha)_i = j, \mathrm{Rad}(\beta_e)_i = \ell, i \in \mathcal{E}_e\}|$ for any $j \in \{\pm 1\}, \ell \in$

$\{\pm 1\}, e \in \mathcal{E}_{tr}$, and then define $\overline{C}_{j\ell} \triangleq \sum_{e\in\mathcal{E}_{tr}} \frac{C^e_{j\ell}}{n_e}$. We can upper bound and formulate $\Delta^t_\Gamma + \Delta^t_\Lambda$ and $\Delta^t_\Gamma - \Delta^t_\Lambda$ as

$$\begin{aligned}
\Delta^t_\Gamma + \Delta^t_\Lambda &\le \frac{2}{m}\left(\frac{\overline{C}_{+1+1}}{1+\exp\left\{2\eta\cdot\sum_{k=0}^{t-1}\left(\Delta^k_\Gamma+\Delta^k_\Lambda\right)\right\}\cdot(1+\delta)^{-1}} - \frac{\overline{C}_{-1-1}}{1+\exp\left\{-2\eta\cdot\sum_{k=0}^{t-1}\left(\Delta^k_\Gamma+\Delta^k_\Lambda\right)\right\}\cdot(1+\delta)}\right)\\
&= \frac{2}{m}\cdot\frac{\overline{C}_{+1+1}(1+\delta) - \overline{C}_{-1-1}\cdot\exp\left\{2\eta\cdot\sum_{k=0}^{t-1}\left(\Delta^k_\Gamma+\Delta^k_\Lambda\right)\right\}}{1+\delta+\exp\left\{2\eta\cdot\sum_{k=0}^{t-1}\left(\Delta^k_\Gamma+\Delta^k_\Lambda\right)\right\}}, \qquad (15)\\
\Delta^t_\Gamma - \Delta^t_\Lambda &\le \frac{2}{m}\left(\frac{\overline{C}_{-1+1}}{1+\exp\left\{2\eta\cdot\sum_{k=0}^{t-1}\left(\Delta^k_\Gamma-\Delta^k_\Lambda\right)\right\}\cdot(1+\delta)^{-1}} - \frac{\overline{C}_{+1-1}}{1+\exp\left\{-2\eta\cdot\sum_{k=0}^{t-1}\left(\Delta^k_\Gamma-\Delta^k_\Lambda\right)\right\}\cdot(1+\delta)}\right)\\
&= \frac{2}{m}\cdot\frac{\overline{C}_{-1+1}(1+\delta) - \overline{C}_{+1-1}\cdot\exp\left\{2\eta\cdot\sum_{k=0}^{t-1}\left(\Delta^k_\Gamma-\Delta^k_\Lambda\right)\right\}}{1+\delta+\exp\left\{2\eta\cdot\sum_{k=0}^{t-1}\left(\Delta^k_\Gamma-\Delta^k_\Lambda\right)\right\}}. \qquad (16)
\end{aligned}$$

Based on similar arguments, we can also establish lower bounds for these two terms,

$$\Delta^t_\Gamma + \Delta^t_\Lambda \ge \frac{2}{m}\cdot\frac{\overline{C}_{+1+1} - \overline{C}_{-1-1}(1+\delta)\cdot\exp\left\{2\eta\cdot\sum_{k=0}^{t-1}\left(\Delta^k_\Gamma+\Delta^k_\Lambda\right)\right\}}{1+\exp\left\{2\eta\cdot\sum_{k=0}^{t-1}\left(\Delta^k_\Gamma+\Delta^k_\Lambda\right)\right\}\cdot(1+\delta)}, \qquad (17)$$

$$\Delta^t_\Gamma - \Delta^t_\Lambda \ge \frac{2}{m}\cdot\frac{\overline{C}_{-1+1} - \overline{C}_{+1-1}(1+\delta)\cdot\exp\left\{2\eta\cdot\sum_{k=0}^{t-1}\left(\Delta^k_\Gamma-\Delta^k_\Lambda\right)\right\}}{1+\exp\left\{2\eta\cdot\sum_{k=0}^{t-1}\left(\Delta^k_\Gamma-\Delta^k_\Lambda\right)\right\}\cdot(1+\delta)}. \qquad (18)$$

The upper and lower bounds (15), (16), (17) and (18) imply that the convergences of $\{\Delta^t_\Gamma + \Delta^t_\Lambda\}$ and $\{\Delta^t_\Gamma - \Delta^t_\Lambda\}$ are determined by recursive equations of the form $\mathcal{Q}^t = \frac{C_1 - C_2\cdot\exp\{\eta\sum_{k=0}^{t-1}\mathcal{Q}^k\}}{1+C_3\cdot\exp\{\eta\sum_{k=0}^{t-1}\mathcal{Q}^k\}}$. We first establish that with suitably chosen η, the sequences $\{\Delta^t_\Gamma + \Delta^t_\Lambda\}$ and $\{\Delta^t_\Gamma - \Delta^t_\Lambda\}$ are guaranteed to be positive. Observed that for the $\mathcal{Q}^t$-type recursive equation, the sign of $\mathcal{Q}^0$ is independent of η, and only determined by the constants C_1, C_2, C_3. At iteration 0, (17) and (18) give

$$\Delta^0_\Gamma + \Delta^0_\Lambda \ge \frac{2}{m}\cdot\frac{\overline{C}_{+1+1} - \overline{C}_{-1-1}(1+\delta)}{2+\delta}, \qquad (19)$$

$$\Delta^0_\Gamma - \Delta^0_\Lambda \ge \frac{2}{m}\cdot\frac{\overline{C}_{-1+1} - \overline{C}_{+1-1}(1+\delta)}{2+\delta}. \qquad (20)$$

To proceed, we need the following concentration lemma to control the deviations of the constants $\overline{C}_{+1+1}, \overline{C}_{+1-1}, \overline{C}_{-1+1}$ and $\overline{C}_{-1-1}$ from their expectations, whose proof is given in Appendix D.2.2.

Lemma D.3. *For $\rho > 0$, considering two environments and denoting $\epsilon_C \triangleq \sqrt{\frac{2\log(16/\rho)}{n}}$, with probability at least $1-\rho$, we have*

$$\begin{aligned}
\left|\overline{C}_{+1+1} - (1-\alpha)(2-\beta_1-\beta_2)\right| &\le \epsilon_C,\\
\left|\overline{C}_{+1-1} - (1-\alpha)(\beta_1+\beta_2)\right| &\le \epsilon_C,\\
\left|\overline{C}_{-1+1} - \alpha(2-\beta_1-\beta_2)\right| &\le \epsilon_C,\\
\left|\overline{C}_{-1-1} - \alpha(\beta_1+\beta_2)\right| &\le \epsilon_C.
\end{aligned} \qquad (21)$$

Using Lemma D.3, with probability at least $1-\rho$, the constants $\overline{C}_{+1+1}, \overline{C}_{+1-1}, \overline{C}_{-1+1}$ and $\overline{C}_{-1-1}$ are close to their expectations.

Based on our assumptions that

$$\alpha, \beta_1, \beta_2 < \frac{1-\epsilon_C-\delta(\frac{1}{4}+\frac{\epsilon_C}{2})}{2} \quad (\alpha, \beta_1, \beta_2 \text{ are sufficiently smaller than } \frac{1}{2}),$$

$$\alpha > \frac{\beta_1+\beta_2}{2} + \epsilon_C + \frac{\delta(1+\epsilon_C)}{2} \quad (\alpha \text{ is sufficiently larger than } \frac{\beta_1+\beta_2}{2}),$$

it can be verified that with probability at least $1-2\rho$, $\Delta_\Gamma^0+\Delta_\Lambda^0>0, \Delta_\Gamma^0-\Delta_\Lambda^0>0$.

Then, at iteration 1, from (17) and (18), we see that as long as we require

$$\eta < \min\left\{\frac{1}{2(\Delta_\Gamma^0+\Delta_\Lambda^0)}\log\frac{\overline{C}_{+1+1}}{\overline{C}_{-1-1}(1+\delta)}, \frac{1}{2(\Delta_\Gamma^0-\Delta_\Lambda^0)}\log\frac{\overline{C}_{-1+1}}{\overline{C}_{+1-1}(1+\delta)}\right\},$$

it holds that $\Delta_\Gamma^1+\Delta_\Lambda^1>0, \Delta_\Gamma^1-\Delta_\Lambda^1>0$. By recursively applying this argument, we see the requirement for η to ensure that $\Delta_\Gamma^t+\Delta_\Lambda^t>0$ and $\Delta_\Gamma^t-\Delta_\Lambda^t>0$ for any $t\in\{0,\dots,T\}$ is

$$\eta < \min\left\{\frac{1}{2\sum_{k=0}^{T-1}(\Delta_\Gamma^k+\Delta_\Lambda^k)}\log\frac{\overline{C}_{+1+1}}{\overline{C}_{-1-1}(1+\delta)}, \frac{1}{2\sum_{k=0}^{T-1}(\Delta_\Gamma^k-\Delta_\Lambda^k)}\log\frac{\overline{C}_{-1+1}}{\overline{C}_{+1-1}(1+\delta)}\right\}. \tag{22}$$

In other words, for the $\mathcal{Q}^t$-type recursive equation, as long as $\mathcal{Q}^0\geq 0$, there always exists a sufficiently small η to guarantee that the whole sequence $\{\mathcal{Q}^t\}$ is positive. From now on, we will focus on the case where the two sequences $\{\Delta_\Gamma^t+\Delta_\Lambda^t\}$ and $\{\Delta_\Gamma^t-\Delta_\Lambda^t\}$ decrease to an $\epsilon_\Delta>0$ error, i.e., $\min_{t\in\{0,\dots,T\}}\{\Delta_\Gamma^t+\Delta_\Lambda^t, \Delta_\Gamma^t-\Delta_\Lambda^t\}=\epsilon_\Delta$.

Then, we show that the two sequences $\{\Delta_\Gamma^t+\Delta_\Lambda^t\}$ and $\{\Delta_\Gamma^t-\Delta_\Lambda^t\}$ decrease monotonically, which thus leads to a more refined upper bound for η at (22). Inspect the upper bounds (15), (16) at iteration $t+1$, which can be written as

$$\Delta_\Gamma^{t+1}+\Delta_\Lambda^{t+1}\leq\frac{2}{m}\cdot\frac{\overline{C}_{+1+1}-\overline{C}_{-1-1}\cdot\exp\left\{2\eta\cdot\sum_{k=0}^{t-1}(\Delta_\Gamma^k+\Delta_\Lambda^k)\right\}\cdot\exp\{2\eta\cdot(\Delta_\Gamma^t+\Delta_\Lambda^t)\}(1+\delta)^{-1}}{1+\exp\left\{2\eta\cdot\sum_{k=0}^{t-1}(\Delta_\Gamma^k+\Delta_\Lambda^k)\right\}\cdot\exp\{2\eta\cdot(\Delta_\Gamma^t+\Delta_\Lambda^t)\}(1+\delta)^{-1}}\triangleq\spadesuit^{t+1},$$

$$\Delta_\Gamma^{t+1}-\Delta_\Lambda^{t+1}\leq\frac{2}{m}\cdot\frac{\overline{C}_{-1+1}-\overline{C}_{+1-1}\cdot\exp\left\{2\eta\cdot\sum_{k=0}^{t-1}(\Delta_\Gamma^k-\Delta_\Lambda^k)\right\}\cdot\exp\{2\eta\cdot(\Delta_\Gamma^t-\Delta_\Lambda^t)\}(1+\delta)^{-1}}{1+\exp\left\{2\eta\cdot\sum_{k=0}^{t-1}(\Delta_\Gamma^k-\Delta_\Lambda^k)\right\}\cdot\exp\{2\eta\cdot(\Delta_\Gamma^t-\Delta_\Lambda^t)\}(1+\delta)^{-1}}\triangleq\clubsuit^{t+1}.$$

Requiring that $\eta>\max\left\{\frac{1}{\Delta_\Gamma^t+\Delta_\Lambda^t}\log(1+\delta), \frac{1}{\Delta_\Gamma^t-\Delta_\Lambda^t}\log(1+\delta)\right\}, \forall t\in\{0,\dots,T\}\Rightarrow\eta>\epsilon_\Delta^{-1}\log(1+\delta)$, we have

$$\begin{aligned}\spadesuit^{t+1}&<\frac{2}{m}\cdot\frac{\overline{C}_{+1+1}-\overline{C}_{-1-1}\cdot\exp\left\{2\eta\cdot\sum_{k=0}^{t-1}(\Delta_\Gamma^k+\Delta_\Lambda^k)\right\}\cdot\exp\{2\eta\cdot(\Delta_\Gamma^t+\Delta_\Lambda^t)\}(1+\delta)^{-1}}{1+\exp\left\{2\eta\cdot\sum_{k=0}^{t-1}(\Delta_\Gamma^k+\Delta_\Lambda^k)\right\}\cdot(1+\delta)}\\&<\Delta_\Gamma^t+\Delta_\Lambda^t,\\\clubsuit^{t+1}&<\frac{2}{m}\cdot\frac{\overline{C}_{-1+1}-\overline{C}_{+1-1}\cdot\exp\left\{2\eta\cdot\sum_{k=0}^{t-1}(\Delta_\Gamma^k-\Delta_\Lambda^k)\right\}\cdot\exp\{2\eta\cdot(\Delta_\Gamma^t-\Delta_\Lambda^t)\}(1+\delta)^{-1}}{1+\exp\left\{2\eta\cdot\sum_{k=0}^{t-1}(\Delta_\Gamma^k-\Delta_\Lambda^k)\right\}\cdot(1+\delta)}\\&<\Delta_\Gamma^t-\Delta_\Lambda^t,\end{aligned}$$

where the last inequalities use the lower bounds (17) and (18).

Based on the above discussion and (22), we can now clarify the requirements of η for the sequences $\{\Delta_\Gamma^t+\Delta_\Lambda^t\}$ and $\{\Delta_\Gamma^t-\Delta_\Lambda^t\}$ to be positive and monotonically decreasing:

$$\begin{aligned}\epsilon_\Delta^{-1}\log(1+\delta)<\eta<\min\Bigg\{&\frac{m(2+\delta)}{4T(\overline{C}_{+1+1}(1+\delta)-\overline{C}_{-1-1})}\log\frac{\overline{C}_{+1+1}}{\overline{C}_{-1-1}(1+\delta)},\\&\frac{m(2+\delta)}{4T(\overline{C}_{-1+1}(1+\delta)-\overline{C}_{+1-1})}\log\frac{\overline{C}_{-1+1}}{\overline{C}_{+1-1}(1+\delta)}\Bigg\},\end{aligned}\tag{23}$$

which uses the upper bounds (15) and (16) at iteration 0. The constants $\overline{C}_{+1+1}$, $\overline{C}_{+1-1}$, $\overline{C}_{-1+1}$ and $\overline{C}_{-1-1}$ can be substituted using the concentration bounds at (21) to generate an upper bound for η that only involves $\alpha,\beta_1,\beta_2,m,\delta,T,\epsilon_C$. Here we omit the precise upper bound for clarity. Note that the left hand side of (23) approaches 0 if $\delta\to 0$, which means that there exists a constant choice of η in (23) if $\underline{n}$ is sufficiently large in Lemma D.2 and D.3.

To conclude, in view of (14), the convergences of the sequences $\{\Delta_\Gamma^t+\Delta_\Lambda^t\}$ and $\{\Delta_\Gamma^t-\Delta_\Lambda^t\}$ imply that $\Lambda_{j,r}^t$ and $\Gamma_{j,r}^t$ are converging, and the positive sequence $\{\Delta_\Gamma^t-\Delta_\Lambda^t\}$ indicates that the increment of the spurious feature $\Gamma_{j,r}^{t+1}-\Gamma_{j,r}^t$ is larger than that of the invariant feature $\Lambda_{j,r}^{t+1}-\Lambda_{j,r}^t$ at any iteration $t\in\{0,\dots,T-1\}$. $\square$

D.2.1. Proof of Lemma D.2

First, we recall some concentration inequalities for sub-Gaussian random variables. Since $\boldsymbol{\xi}_i^e \sim \mathcal{N}(0, \sigma_p^2 \cdot (\mathbf{I}_d - \mathbf{v}_1\mathbf{v}_1^\top - \mathbf{v}_2\mathbf{v}_2^\top))$, for $(i', e') \neq (i, e)$, using Bernstein's inequality for sub-exponential random variables, we have for sufficiently small $a \geq 0$,

$$\Pr\left\{|\langle \boldsymbol{\xi}_i^e, \boldsymbol{\xi}_{i'}^{e'}\rangle| \geq a\right\} \leq 2\exp\left\{-\frac{a^2}{4\sigma_p^4(d-2)}\right\},$$

$$\Pr\left\{\left|\|\boldsymbol{\xi}_i^e\|_2^2 - \sigma_p^2(d-2)\right| \geq a\right\} \leq 2\exp\left\{-\frac{a^2}{512\sigma_p^4(d-2)}\right\}.$$

Moreover, for $\xi_r \sim \mathcal{N}(0, \sigma_0^2)$ (indicating the initial weights $\mathbf{w}_{j,r}^0$), the standard Gaussian tail gives

$$\Pr\left\{\left|\frac{1}{m}\sum_{r=1}^m \xi_r\right| \geq a\right\} \leq 2\exp\left\{-\frac{ma^2}{2\sigma_0^2}\right\}.$$

Denote $n \triangleq \sum_{e\in\mathcal{E}_{tr}} n_e$, $\underline{n} \triangleq \min_{e\in\mathcal{E}_{tr}} n_e$, by properly choosing a for each tail bound and applying a union bound, we can conclude that for $\rho > 0$, with probability at least $1-\rho$, it holds that $\forall i, e, i', e', r$,

$$|\langle \boldsymbol{\xi}_i^e, \boldsymbol{\xi}_{i'}^{e'}\rangle| \leq 2\sigma_p^2\sqrt{(d-2)\log\frac{8n^2}{\rho}}, \quad \|\boldsymbol{\xi}_i^e\|_2^2 \leq \sigma_p^2(d-2) + 16\sigma_p^2\sqrt{2(d-2)\log\frac{8n}{\rho}},$$

$$\left|\frac{1}{m}\sum_{r=1}^m \xi_r\right| \leq \sigma_0\sqrt{\frac{2}{m}\log\frac{32m}{\rho}}, \qquad |\langle \boldsymbol{\xi}_r, \boldsymbol{\xi}_{i'}^{e'}\rangle| \leq 2\sigma_p\sigma_0\sqrt{(d-2)\log\frac{16nm}{\rho}}.$$

We start with bound the growth of $\Xi_{j,r,i}^{t,e}$. By bounding the update rule (13), with probability at least $1-\rho$, we have

$$\begin{aligned}
\left|\Xi_{j,r,i'}^{t+1,e'}\right| &\leq \left|\Xi_{j,r,i'}^{t,e'}\right| + \frac{\eta}{m}\sum_{e\in\mathcal{E}_{tr}}\frac{1}{n_e}\sum_{i=1}^{n_e}\frac{1}{1+\exp\{y_i^e\hat{y}_i^e\}}\cdot|\langle \boldsymbol{\xi}_i^e, \boldsymbol{\xi}_{i'}^{e'}\rangle| \\
&\leq \left|\Xi_{j,r,i'}^{t,e'}\right| + \frac{\eta}{m}\sum_{e\in\mathcal{E}_{tr}}\frac{1}{n_e}\sum_{i=1}^{n_e}|\langle \boldsymbol{\xi}_i^e, \boldsymbol{\xi}_{i'}^{e'}\rangle| \\
&= \left|\Xi_{j,r,i'}^{0,e'}\right| + (t+1)\cdot\frac{\eta}{m}\sum_{e\in\mathcal{E}_{tr}}\frac{1}{n_e}\sum_{i=1}^{n_e}|\langle \boldsymbol{\xi}_i^e, \boldsymbol{\xi}_{i'}^{e'}\rangle| \\
&= |\langle \boldsymbol{\xi}_r, \boldsymbol{\xi}_{i'}^{e'}\rangle| + (t+1)\cdot\left(\frac{\eta}{mn_{e'}}\|\boldsymbol{\xi}_{i'}^{e'}\|_2^2 + \sum_{(i,e)\neq(i',e')}\frac{\eta}{mn_e}|\langle \boldsymbol{\xi}_i^e, \boldsymbol{\xi}_{i'}^{e'}\rangle|\right) \\
&\leq 2\sigma_p\sigma_0\sqrt{(d-2)\log\frac{16nm}{\rho}} \\
&\quad + \frac{T\eta\sigma_p^2}{m\underline{n}}\left((d-2) + 16\sqrt{2(d-2)\log\frac{8n}{\rho}} + 2n\sqrt{(d-2)\log\frac{8n^2}{\rho}}\right).
\end{aligned}$$

Then, we can bound $|\mathbb{Q}_i^e|$ as

$$\begin{aligned}
|\mathbb{Q}_i^e| &\leq 2\cdot\left|\frac{1}{m}\sum_{r=1}^m \xi_r\right| + 2\cdot\left|\frac{1}{m}\sum_{r=1}^m \xi_r\right| + \frac{2}{m}\sum_{r=1}^m\left|\Xi_{j,r,i}^{t,e}\right| \\
&\leq 4\sigma_0\sqrt{\frac{2}{m}\log\frac{32m}{\rho}} + 4\sigma_p\sigma_0\sqrt{(d-2)\log\frac{16nm}{\rho}} \\
&\quad + \frac{2T\eta\sigma_p^2}{m\underline{n}}\left((d-2) + 16\sqrt{2(d-2)\log\frac{8n}{\rho}} + 2n\sqrt{(d-2)\log\frac{8n^2}{\rho}}\right).
\end{aligned}$$

Thus, with sufficient small σ_0, σ_p, i.e.,

$$\sigma_0^2 = O\left(\underline{n}^{-2} \log^{-1}(m/\rho)\right),$$
$$\sigma_p^2 = O\left(\min\left\{d^{-1/2} \log^{-1/2}(nm/\rho), T^{-1}\eta^{-1}m\left(d + n\sqrt{d\log(n^2/\rho)}\right)^{-1}\right\}\right),$$

we ensured that $|\mathbb{Q}_i^e| = O(\underline{n}^{-1})$.

D.2.2. Proof of Lemma D.3

For $e \in \mathcal{E}_{tr}$, using Hoeffding's inequality, it holds that

$$\Pr\left\{\left|\frac{1}{n_e}\sum_{i=1}^{n_e} \mathbf{1}_{\{\mathrm{Rad}(\alpha)_i=+1, \mathrm{Rad}(\beta_e)_i=+1\}} - (1-\alpha)(1-\beta_e)\right| \geq a\right\} \leq 2\exp\{-2a^2 n_e\}.$$

Considering two environments, using a union bound, we can conclude that

$$\Pr\left\{\left|\overline{C}_{+1+1} - (1-\alpha)(2-\beta_1-\beta_2)\right| \leq a\right\} \geq 1 - 4\exp\left\{-\frac{a^2\underline{n}}{2}\right\}.$$

Thus, for $\rho > 0$, with probability at least $1 - \frac{\rho}{4}$, we can conclude that

$$\left|\overline{C}_{+1+1} - (1-\alpha)(2-\beta_1-\beta_2)\right| \leq \sqrt{\frac{2\log(16/\rho)}{\underline{n}}}.$$

Using the above arguments for other constants $\overline{C}_{+1-1}$, $\overline{C}_{-1+1}$ and $\overline{C}_{-1-1}$, and applying a union bound, we obtain the desired results.

D.3. Proof for Theorem 3.2

Theorem D.4 (Restatement of Theorem 3.2)**.** *Consider training a CNN model with the same data as in Theorem 3.1, define*

$$\mathbf{c}(t) \triangleq \left[C^1_{\textit{IRMv1}}(\mathbf{W},t), C^2_{\textit{IRMv1}}(\mathbf{W},t), \cdots, C^{|\mathcal{E}_{tr}|}_{\textit{IRMv1}}(\mathbf{W},t)\right],$$

and $\lambda_0 = \lambda_{\min}(\mathbf{H}^\infty)$, *where* $\mathbf{H}^\infty_{e,e'} \triangleq \frac{1}{2mn_e n_{e'}} \sum_{i=1}^{n_e} \mathbf{x}^{e\top}_{1,i} \sum_{i'=1}^{n_{e'}} \mathbf{x}^{e'}_{1,i}$. *Suppose that dimension* $d = \Omega(\log(m/\delta))$, *network width* $m = \Omega(1/\delta)$, *regularization factor* $\lambda \geq 1/\sigma_0$, *noise variance* $\sigma_p = O(d^{-2})$, *weight initial scale* $\sigma_0 = O(\min\{\frac{\lambda_0^2 m^2}{\log(1/\epsilon)}, \frac{\lambda_0 m}{\sqrt{d}\log(1/\epsilon)}\})$, *then with probability at least* $1-\delta$, *after training time* $T = \Omega\left(\frac{\log(1/\epsilon)}{\eta\lambda\lambda_0}\right)$, *we have:*

$$\|\mathbf{c}(T)\|_2 \leq \epsilon, \quad \gamma_{j,r,1}(T) = o_d(1), \quad \gamma_{j,r,2}(T) = o_d(1).$$

Before proving Theorem D.4, we first provide some useful lemmas as follows:

Lemma D.5. *Suppose that* $\delta > 0$ *and* $d = \Omega(\log(4n/\delta))$. *Then with probability at least* $1-\delta$,

$$\sigma_p^2 d/2 \leq \|\boldsymbol{\xi}_i\|_2^2 \leq 3\sigma_p^2 d/2$$

for all $i, i' \in [n]$.

Proof of Lemma D.5. By Bernstein's inequality, with probability at least $1-\delta/(2n)$ we have

$$\left|\|\boldsymbol{\xi}_i\|_2^2 - \sigma_p^2 d\right| = O(\sigma_p^2 \cdot \sqrt{d\log(4n/\delta)}).$$

Therefore, as long as $d = \Omega(\log(4n/\delta))$, we have

$$\sigma_p^2 d/2 \leq \|\boldsymbol{\xi}_i\|_2^2 \leq 3\sigma_p^2 d/2.$$

□

Lemma D.6. *Suppose that* $d \geq \Omega(\log(mn/\delta))$, $m = \Omega(\log(1/\delta))$. *Then with probability at least* $1-\delta$,

$$|\langle \mathbf{w}^{(0)}_{j,r}, \mathbf{v}_1\rangle| \leq \sqrt{2\log(8m/\delta)} \cdot \sigma_0 \|\mathbf{v}_1\|_2,$$
$$|\langle \mathbf{w}^{(0)}_{j,r}, \mathbf{v}_2\rangle| \leq \sqrt{2\log(8m/\delta)} \cdot \sigma_0 \|\mathbf{v}_2\|_2,$$
$$|\langle \mathbf{w}^{(0)}_{j,r}, \boldsymbol{\xi}_i\rangle| \leq 2\sqrt{\log(8mn/\delta)} \cdot \sigma_0 \sigma_p \sqrt{d}$$

for all $r \in [m]$, $j \in \{\pm 1\}$ *and* $i \in [n]$.

Proof of Lemma D.6. It is clear that for each $r \in [m]$, $j \cdot \langle \mathbf{w}^{(0)}_{j,r}, \mathbf{v}_1\rangle$ is a Gaussian random variable with mean zero and variance $\sigma_0^2\|\mathbf{v}_1\|_2^2$. Therefore, by Gaussian tail bound and union bound, with probability at least $1-\delta$,

$$j \cdot \langle \mathbf{w}^{(0)}_{j,r}, \mathbf{v}_1\rangle \leq |\langle \mathbf{w}^{(0)}_{j,r}, \mathbf{v}_1\rangle| \leq \sqrt{2\log(8m/\delta)} \cdot \sigma_0 \|\mathbf{v}_1\|_2.$$

Similarly, we have

$$j \cdot \langle \mathbf{w}^{(0)}_{j,r}, \mathbf{v}_2\rangle \leq |\langle \mathbf{w}^{(0)}_{j,r}, \mathbf{v}_2\rangle| \leq \sqrt{2\log(8m/\delta)} \cdot \sigma_0 \|\mathbf{v}_2\|_2.$$

By Lemma D.5, with probability at least $1-\delta$, $\sigma_p\sqrt{d}/\sqrt{2} \leq \|\boldsymbol{\xi}_i\|_2 \leq \sqrt{3/2} \cdot \sigma_p\sqrt{d}$ for all $i \in [n]$. Therefore, the result for $\langle \mathbf{w}^{(0)}_{j,r}, \boldsymbol{\xi}_i\rangle$ follows the same proof as $j \cdot \langle \mathbf{w}^{(0)}_{j,r}, \mathbf{v}_1\rangle$. □

Proof. The proof is by induction method. First we show the gradient flow of weights by IRMv1 objective function (3):

$$
\begin{aligned}
\frac{d\mathbf{w}_{j,r}(t)}{dt} &= -\eta \cdot \nabla_{\mathbf{w}_{j,r}} L_{\mathrm{IRMv1}}(\mathbf{W}(t)) \\
&= -\frac{\eta}{nm} \cdot \sum_{e\in\mathcal{E}_{\mathrm{tr}}} \sum_{i=1}^{n_e} \ell_i'(t)\sigma'(\langle \mathbf{w}_{j,r}(t), y_i^e \mathbf{v}_i^e\rangle) \cdot j\mathbf{v}_i^e - \frac{\eta}{nm} \cdot \sum_{e\in\mathcal{E}_{\mathrm{tr}}} \sum_{i=1}^{n_e} \ell_i'(t)\sigma'(\langle \mathbf{w}_{j,r}(t), \boldsymbol{\xi}_i\rangle) \cdot j y_i^e \boldsymbol{\xi}_i \\
&\quad - \frac{\eta\lambda}{nm} \cdot \sum_{e\in\mathcal{E}_{\mathrm{tr}}} C_{\mathrm{IRMv1}}^e \sum_{i=1}^{n_e} \ell_i'' \hat{y}_i^e \sigma'(\langle \mathbf{w}_{j,r}(t), y_i^e \mathbf{v}_i^e\rangle) \cdot j y_i^e \mathbf{v}_i^e - \frac{\eta\lambda}{nm} \cdot \sum_{e\in\mathcal{E}_{\mathrm{tr}}} C_{\mathrm{IRMv1}}^e \sum_{i=1}^{n_e} \ell_i'' \hat{y}_i^e \sigma'(\langle \mathbf{w}_{j,r}(t), \boldsymbol{\xi}_i\rangle) \cdot j \boldsymbol{\xi}_i \\
&\quad - \frac{\eta\lambda}{nm} \cdot \sum_{e\in\mathcal{E}_{\mathrm{tr}}} C_{\mathrm{IRMv1}}^e \sum_{i=1}^{n_e} \ell_i'(t)\sigma'(\langle \mathbf{w}_{j,r}(t), y_i^e \mathbf{v}_i^e\rangle) \cdot j\mathbf{v}_i^e - \frac{\eta\lambda}{nm} \cdot \sum_{e\in\mathcal{E}_{\mathrm{tr}}} C_{\mathrm{IRMv1}}^e \sum_{i=1}^{n_e} \ell_i'(t)\sigma'(\langle \mathbf{w}_{j,r}(t), \boldsymbol{\xi}_i\rangle) \cdot j y_i^e \boldsymbol{\xi}_i \\
&= -\frac{\eta}{nm} \cdot \sum_{e\in\mathcal{E}_{\mathrm{tr}}} (1+2\lambda C_{\mathrm{IRMv1}}^e(t)) \sum_{i=1}^{n_e} \ell_i'(t)\sigma'(\langle \mathbf{w}_{j,r}(t), y_i^e \mathbf{v}_i^e\rangle) \cdot j\mathbf{v}_i^e \\
&\quad - \frac{\eta}{nm} \cdot \sum_{e\in\mathcal{E}_{\mathrm{tr}}} (1+2\lambda C_{\mathrm{IRMv1}}^e(t)) \sum_{i=1}^{n_e} \ell_i'(t)\sigma'(\langle \mathbf{w}_{j,r}(t), \boldsymbol{\xi}_i\rangle) \cdot j y_i^e \boldsymbol{\xi}_i \\
&\quad - \frac{\eta\lambda}{nm} \cdot \sum_{e\in\mathcal{E}_{\mathrm{tr}}} C_{\mathrm{IRMv1}}^e \sum_{i=1}^{n_e} \ell_i'' \hat{y}_i^e \sigma'(\langle \mathbf{w}_{j,r}(t), y_i^e \mathbf{v}_i^e\rangle) \cdot j y_i^e \mathbf{v}_i^e - \frac{\eta\lambda}{nm} \cdot \sum_{e\in\mathcal{E}_{\mathrm{tr}}} C_{\mathrm{IRMv1}}^e \sum_{i=1}^{n_e} \ell_i'' \hat{y}_i^e \sigma'(\langle \mathbf{w}_{j,r}(t), \boldsymbol{\xi}_i\rangle) \cdot j \boldsymbol{\xi}_i,
\end{aligned}
$$

where $C_{\mathrm{IRMv1}}^e = \frac{1}{n_e}\sum_{i=1}^{n_e} \ell_i' \hat{y}_i^e y_i^e$ and $\mathbf{v}_i^e = \mathrm{Rad}(\alpha)_i \cdot \mathbf{v}_1 + \mathrm{Rad}(\beta_e)_i \cdot \mathbf{v}_2$. Note that ℓ'' has the opposite sign to ℓ'.

Then we look at the dynamics of $C_{\mathrm{IRMv1}}^e(t)$ according to the gradient flow update rule:

$$
\begin{aligned}
\frac{dC_{\mathrm{IRMv1}}^e(\mathbf{W},t)}{dt} &= \sum_{j=\pm1}\sum_{r=1}^{m} \left\langle \frac{\partial C_{\mathrm{IRMv1}}^e(\mathbf{W},t)}{\partial \mathbf{w}_{j,r}(t)}, \frac{d\mathbf{w}_{j,r}(t)}{dt} \right\rangle \\
&= \sum_{e'} 2\lambda C_{\mathrm{IRMv1}}^{e'}(\mathbf{W},t) \sum_{j}\sum_{r=1}^{m} \left\langle \frac{\partial C_{\mathrm{IRMv1}}^e(\mathbf{W},t)}{\partial \mathbf{w}_{j,r}(t)}, \frac{\partial C_{\mathrm{IRMv1}}^{e'}(\mathbf{W},t)}{\partial \mathbf{w}_{j,r}(t)} \right\rangle + \\
&\quad \sum_{j=\pm1}\sum_{r=1}^{m} \left\langle \frac{\partial C_{\mathrm{IRMv1}}^e(\mathbf{W},t)}{\partial \mathbf{w}_{j,r}(t)}, \frac{\partial L_s(\mathbf{W},t)}{\partial \mathbf{w}_{j,r}(t)} \right\rangle \\
&= 2\lambda \sum_{e'} C_{\mathrm{IRMv1}}^{e'}(\mathbf{W},t) \cdot \mathbf{H}_{e,e'}(t) + \mathbf{g}_e(t),
\end{aligned}
$$

where we define $\mathbf{H}_{e,e'}(t) = \sum_j \sum_{r=1}^m \left\langle \frac{\partial C_{\mathrm{IRMv1}}^e(\mathbf{W},t)}{\partial \mathbf{w}_{j,r}(t)}, \frac{\partial C_{\mathrm{IRMv1}}^{e'}(\mathbf{W},t)}{\partial \mathbf{w}_{j,r}(t)} \right\rangle$ and $\mathbf{g}_e(t) = \sum_{j=\pm1}\sum_{r=1}^m \left\langle \frac{\partial C_{\mathrm{IRMv1}}^e(\mathbf{W},t)}{\partial \mathbf{w}_{j,r}(t)}, \frac{\partial L_s(\mathbf{W},t)}{\partial \mathbf{w}_{j,r}(t)} \right\rangle$. Thus $\mathbf{H}(t)$ is an $|\mathcal{E}_{\mathrm{tr}}|\times|\mathcal{E}_{\mathrm{tr}}|$ matrix. We can write the dynamics of $\mathbf{c}(t) = \left[C_{\mathrm{IRMv1}}^1(\mathbf{W},t), C_{\mathrm{IRMv1}}^2(\mathbf{W},t), \cdots, C_{\mathrm{IRMv1}}^{|\mathcal{E}_{\mathrm{tr}}|}(\mathbf{W},t)\right]$ in a compact way:

$$
\frac{d\mathbf{c}(t)}{dt} = 2\lambda \cdot \mathbf{H}(t)\mathbf{c}(t) + \mathbf{g}(t).
$$

Our next step is to show $\mathbf{H}(t)$ is stable in terms of $\mathbf{W}(t)$. To proceed with the analysis, we write down the expression for $\frac{\partial C_{\mathrm{IRMv1}}^e(\mathbf{W},t)}{\partial \mathbf{w}_{j,r}(t)} \in \mathbb{R}^d$:

$$
\begin{aligned}
\frac{\partial C_{\mathrm{IRMv1}}^e(\mathbf{W}(t))}{\partial \mathbf{w}_{j,r}(t)} &= \frac{\eta}{n_e m} \cdot \sum_{i=1}^{n_e} \ell_i'(t)\sigma'(\langle \mathbf{w}_{j,r}(t), y_i^e \mathbf{v}_i^e\rangle) \cdot j\mathbf{v}_i^e + \frac{\eta}{n_e m} \sum_{i=1}^{n_e} \ell_i'(t)\sigma'(\langle \mathbf{w}_{j,r}(t), \boldsymbol{\xi}_i\rangle) \cdot j y_i^e \boldsymbol{\xi}_i \\
&\quad + \frac{\eta}{n_e m} \cdot \sum_{i=1}^{n_e} \ell_i'' y_i^e \sigma'(\langle \mathbf{w}_{j,r}(t), y_i^e \mathbf{v}_i^e\rangle) \cdot j y_i^e \mathbf{v}_i^e + \frac{\eta}{n_e m} \cdot \sum_{i=1}^{n_e} \ell_i'' y_i^e \sigma'(\langle \mathbf{w}_{j,r}(t), \boldsymbol{\xi}_i\rangle) \cdot j \boldsymbol{\xi}_i.
\end{aligned}
$$

When we consider linear activation function $\sigma(x) = x$, the entry of matrix $\mathbf{H}(t)$ reduces to:

$$
\begin{aligned}
\mathbf{H}_{e,e'}(t) &= \sum_j \sum_{r=1}^m \left\langle \frac{\partial C^e_{\text{IRMv1}}(\mathbf{W},t)}{\partial \mathbf{w}_{j,r}(t)}, \frac{\partial C^{e'}_{\text{IRMv1}}(\mathbf{W},t)}{\partial \mathbf{w}_{j,r}(t)} \right\rangle \\
&= \sum_j \sum_{r=1}^m \left(\frac{1}{n_e m}\right)\left(\frac{1}{n_{e'} m}\right) \left[\sum_{i=1}^{n_e} \ell_i'(t) \cdot j\mathbf{v}_i^{e\top} \sum_{i=1}^{n_{e'}} \ell_i'(t) \cdot j\mathbf{v}_i^e + \sum_{i=1}^{n_e} \ell_i''(t) y_i^e(t) \cdot j y_i^e \mathbf{v}_i^{e\top} \sum_{i=1}^{n_{e'}} \ell_i''(t) y_i^e(t) \cdot j y_i^e \mathbf{v}_i^e \right] \\
&+ \sum_j \sum_{r=1}^m \left(\frac{1}{n_e m}\right)\left(\frac{1}{n_{e'} m}\right) \left[\sum_{i=1}^{n_e} \ell_i''(t) \hat{y}_i^e(t) \cdot j y_i^e \mathbf{v}_i^{e\top} \sum_{i=1}^{n_{e'}} \ell_i'(t) \cdot j\mathbf{v}_i^e + \sum_{i=1}^{n_e} \ell_i'(t) \cdot j\mathbf{v}_i^{e\top} \sum_{i=1}^{n_{e'}} \ell_i''(t) \hat{y}_i^e(t) \cdot j\mathbf{v}_i^e \right] \\
&+ \sum_j \sum_{r=1}^m \left(\frac{1}{n_e m}\right)\left(\frac{1}{n_{e'} m}\right) \left[\sum_{i=1}^{n_e} \ell_i'(t) \cdot j y_i^e \boldsymbol{\xi}_i^{e\top} \sum_{i=1}^{n_{e'}} \ell_i'(t) \cdot j y_i^e \boldsymbol{\xi}_i^e + \sum_{i=1}^{n_e} \ell_i''(t) y_i^e(t) \cdot j \boldsymbol{\xi}_i^{e\top} \sum_{i=1}^{n_{e'}} \ell_i''(t) \cdot j \boldsymbol{\xi}_i^e \right] \\
&+ \sum_j \sum_{r=1}^m \left(\frac{1}{n_e m}\right)\left(\frac{1}{n_{e'} m}\right) \left[\sum_{i=1}^{n_e} \ell_i''(t) \cdot j \boldsymbol{\xi}_i^{e\top} \sum_{i=1}^{n_{e'}} \ell_i'(t) \cdot j y_i^e \boldsymbol{\xi}_i^e + \sum_{i=1}^{n_e} y_i^e \ell_i'(t) \cdot j \boldsymbol{\xi}_i^{e\top} \sum_{i=1}^{n_{e'}} \ell_i''(t) \cdot j \boldsymbol{\xi}_i^e \right] \\
&\triangleq \mathbf{H}^1_{e,e'}(t) + \mathbf{H}^2_{e,e'}(t) + \mathbf{H}^3_{e,e'}(t) + \mathbf{H}^4_{e,e'}(t) + \mathbf{H}^5_{e,e'}(t) + \mathbf{H}^6_{e,e'}(t) + \mathbf{H}^7_{e,e'}(t) + \mathbf{H}^8_{e,e'}(t).
\end{aligned}
$$

Define

$$
\begin{aligned}
\mathbf{H}^{1,\infty}_{e,e'} &= \sum_j \sum_{r=1}^m \left(\frac{1}{n_e m}\right)\left(\frac{1}{n_{e'} m}\right) \left[\sum_{i=1}^{n_e} -\frac{1}{2} \cdot j\mathbf{v}_i^{e\top} \sum_{i=1}^{n_{e'}} -\frac{1}{2} \cdot j\mathbf{v}_i^e \right] \\
&= \frac{1}{2mn_e n_{e'}} \sum_{i=1}^{n_e} \mathbf{v}_i^{e\top} \sum_{i'=1}^{n_{e'}} \mathbf{v}_i^{e'}.
\end{aligned}
$$

Then we can show that

$$
\begin{aligned}
\left|\mathbf{H}^1_{e,e'}(t) - \mathbf{H}^{1,\infty}_{e,e'}\right| &= \frac{2}{mn_e n_{e'}} \left| \sum_{i=1}^{n_e} \ell_i'(t)\mathbf{v}_i^{e\top} \sum_{i'=1}^{n_{e'}} \ell_i'(t)\mathbf{v}_i^{e'} - \sum_{i=1}^{n_e} \frac{1}{2}\mathbf{v}_i^{e\top} \sum_{i'=1}^{n_{e'}} \frac{1}{2}\mathbf{v}_i^{e'} \right| \\
&\le \frac{2}{mn_e n_{e'}} \left| \sum_{i=1}^{n_e} \ell_i'(t)\mathbf{v}_i^{e\top} \sum_{i'=1}^{n_{e'}} \ell_i'(t)\mathbf{v}_i^{e'} - \sum_{i=1}^{n_e} \ell_i'\mathbf{v}_i^{e\top} \sum_{i'=1}^{n_{e'}} \frac{1}{2}\mathbf{v}_i^{e'} \right| \\
&\quad + \frac{2}{mn_e n_{e'}} \left| \sum_{i=1}^{n_e} \ell_i'(t)\mathbf{v}_i^{e\top} \sum_{i'=1}^{n_{e'}} \frac{1}{2}\mathbf{v}_i^{e'} - \sum_{i=1}^{n_e} \frac{1}{2}\mathbf{v}_i^{e\top} \sum_{i'=1}^{n_{e'}} \frac{1}{2}\mathbf{v}_i^{e'} \right| \\
&\le \frac{2}{mn_e n_{e'}} \left| \sum_{i=1}^{n_e} \ell_i'(t)\mathbf{v}_i^{e\top} \sum_{i'=1}^{n_{e'}} \left(\ell_i'(t) + \frac{1}{2}\right)\mathbf{v}_i^{e'} \right| + \frac{2}{mn_e n_{e'}} \left| \sum_{i=1}^{n_e} \left(\ell_i'(t) + \frac{1}{2}\right)\mathbf{v}_i^{e\top} \sum_{i'=1}^{n_{e'}} \frac{1}{2}\mathbf{v}_i^{e'} \right| \\
&\le C\frac{2\gamma}{m},
\end{aligned}
$$

where C is an absolute constant, γ is defined as follows:

$$
|\hat{y}_i^e(t)| = |f(\mathbf{x}_i, t)| = \left| \frac{1}{m} \sum_j \sum_{r=1}^m \left[\sigma(\mathbf{w}_{j,r}^\top(t)\mathbf{x}_1) + \sigma(\mathbf{w}_{j,r}^\top(t)\mathbf{x}_2)\right] \right| \le \gamma,
$$

and we have used the bound for $\ell_i'(t)+\frac{1}{2}$:

$$\begin{aligned}\left|\ell_i'(t)+\frac{1}{2}\right| &= \left|-\frac{\exp(-y_i^e\cdot f(\mathbf{W},\mathbf{x}_i,t))}{1+\exp(-y_i^e\cdot f(\mathbf{W},\mathbf{x}_i,t))}+\frac{1}{2}\right| \\ &= \left|\frac{1}{2}-\frac{1}{1+\exp(y_i^e\cdot f(\mathbf{W},\mathbf{x}_i,t))}\right| \\ &\le \max\left\{\left|\frac{1}{2}-\frac{1}{1+\exp(\gamma)}\right|,\left|\frac{1}{2}-\frac{1}{1+\exp(-\gamma)}\right|\right\} \\ &\le \max\left\{\left|\frac{1}{2}-\frac{1}{2+\frac{7}{4}\gamma}\right|,\left|\frac{1}{2}-\frac{1}{2-\gamma}\right|\right\}=\Theta(\gamma).\end{aligned}$$

and we provide the bound of $\ell_i''(t)-\frac{1}{4}$:

$$\begin{aligned}\left|\ell_i''(t)-\frac{1}{4}\right| &= \left|\frac{\exp(-y_i^e\cdot f(\mathbf{W},\mathbf{x}_i,t))}{(1+\exp(-y_i^e\cdot f(\mathbf{W},\mathbf{x}_i,t)))^2}-\frac{1}{4}\right| \\ &= \left|\frac{1}{\exp(y_i^e\cdot f(\mathbf{W},\mathbf{x}_i,t))+2+\exp(-y_i^e\cdot f(\mathbf{W},\mathbf{x}_i,t))}-\frac{1}{4}\right| \\ &\le \left|\frac{1}{4}-\frac{1}{2+2\exp(\gamma^2/2)}\right|=\Theta(\gamma^2).\end{aligned}$$

Similarly, we have:

$$\begin{aligned}\left|\mathbf{H}^2_{e,e'}(t)\right| &= \frac{2}{mn_en_{e'}}\left|\sum_{i=1}^{n_e}\ell_i''(t)\hat{y}_i^e(t)\cdot jy_i^e\mathbf{v}_i^{e\top}\sum_{i=1}^{n_{e'}}\ell_i''(t)\hat{y}_i^e(t)\cdot jy_i^e\mathbf{v}_i^e\right|\le C\frac{2\gamma^2}{m}, \\ \left|\mathbf{H}^3_{e,e'}(t)\right| &= \frac{2}{mn_en_{e'}}\left|\sum_{i=1}^{n_e}\ell_i''(t)\hat{y}_i^e(t)\cdot jy_i^e\mathbf{v}_i^{e\top}\sum_{i=1}^{n_{e'}}\ell_i'(t)\cdot j\mathbf{v}_i^e\right|\le C\frac{2\gamma}{m}, \\ \left|\mathbf{H}^4_{e,e'}(t)\right| &= \frac{2}{mn_en_{e'}}\left|+\sum_{i=1}^{n_e}\ell_i'(t)\cdot j\mathbf{v}_i^{e\top}\sum_{i=1}^{n_{e'}}\ell_i''(t)\hat{y}_i^e(t)\cdot j\mathbf{v}_i^e\right|\le C\frac{2\gamma}{m}, \\ \left|\mathbf{H}^5_{e,e'}(t)\right| &= \frac{2}{mn_en_{e'}}\left|\sum_{i=1}^{n_e}\ell_i'(t)\cdot jy_i^e\boldsymbol{\xi}_i^{e\top}\sum_{i=1}^{n_{e'}}\ell_i'(t)\cdot jy_i^e\boldsymbol{\xi}_i^e\right|\le C\frac{2}{m}\sigma_q^2d, \\ \left|\mathbf{H}^6_{e,e'}(t)\right| &= \frac{2}{mn_en_{e'}}\left|\sum_{i=1}^{n_e}\ell_i''(t)y_i^e(t)\cdot j\boldsymbol{\xi}_i^{e\top}\sum_{i=1}^{n_{e'}}\ell_i''(t)\cdot j\boldsymbol{\xi}_i^e\right|\le C\frac{2}{m}\sigma_q^2d\gamma^2, \\ \left|\mathbf{H}^7_{e,e'}(t)\right| &= \frac{2}{mn_en_{e'}}\left|\sum_{i=1}^{n_e}\ell_i''(t)\cdot j\boldsymbol{\xi}_i^{e\top}\sum_{i=1}^{n_{e'}}\ell_i'(t)\cdot jy_i^e\boldsymbol{\xi}_i^e\right|\le C\frac{2}{m}\sigma_q^2d\gamma, \\ \left|\mathbf{H}^8_{e,e'}(t)\right| &= \frac{2}{mn_en_{e'}}\left|\sum_{i=1}^{n_e}y_i^e\ell_i'(t)\cdot j\boldsymbol{\xi}_i^{e\top}\sum_{i=1}^{n_{e'}}\ell_i''(t)\cdot j\boldsymbol{\xi}_i^e\right|\le C\frac{2}{m}\sigma_q^2d\gamma.\end{aligned}$$

To summarize, we have that,

$$\left|\mathbf{H}_{e,e'}(t)-\mathbf{H}^\infty_{e,e'}\right|\le C_1\frac{2}{m}\gamma+C_2\frac{2}{m}\sigma_q^2\gamma.$$

Furthermore, we have that

$$|\mathbf{g}_e(t)|\le C\frac{2}{m}\max\{\sigma_q^2d,\gamma\}.$$

Finally, we have the dynamics for $\|\mathbf{c}(t)\|_2^2$

$$\frac{d\|\mathbf{c}(t)\|_2^2}{dt}=-2\lambda\mathbf{c}^\top(t)\mathbf{H}(t)\mathbf{c}(t)-\mathbf{c}(t)\mathbf{g}(t)\le-\lambda_0\lambda\|\mathbf{c}(t)\|_2^2,$$

which requires that:

$$C_1 \frac{2}{m}\gamma < \lambda_0; \quad \lambda > \frac{1}{\|\mathbf{c}(0)\|_2}.$$

According to the gradient descent for IRMV1 objective function, the evolution of coefficients can be expressed as:

$$\begin{aligned}
\gamma_{j,r,1}(t+1) = \gamma_{j,r,1}(t) - \frac{\eta}{m} \cdot \sum_{e\in\mathcal{E}_{\rm tr}} (1 + 2\lambda C^e_{\text{IRMv1}}(t)) \frac{1}{n_e} \sum_{i=1}^{n_e} \ell'_i(t) \mathrm{Rad}(\alpha)_i \\
- \frac{\eta\lambda}{m} \cdot \sum_{e\in\mathcal{E}_{\rm tr}} 2C^e_{\text{IRMv1}} \frac{1}{n_e} \sum_{i=1}^{n_e} \ell''_i \hat{y}^e_i \cdot y^e_i \mathrm{Rad}(\alpha)_i, \\
\gamma_{j,r,2}(t+1) = \gamma_{j,r,2}(t) - \frac{\eta}{m} \cdot \sum_{e\in\mathcal{E}_{\rm tr}} (1 + 2\lambda C^e_{\text{IRMv1}}(t)) \frac{1}{n_e} \sum_{i=1}^{n_e} \ell'_i(t) \mathrm{Rad}(\beta_e) \\
- \frac{\eta\lambda}{m} \cdot \sum_{e\in\mathcal{E}_{\rm tr}} 2C^e_{\text{IRMv1}} \frac{1}{n_e} \sum_{i=1}^{n_e} \ell''_i \hat{y}^e_i \cdot y^e_i \mathrm{Rad}(\beta_e)_i.
\end{aligned}$$

Then we have,

$$\begin{aligned}
|\gamma_{j,r,1}(t+1)| &\le |\gamma_{j,r,1}(t)| + \left| \frac{\eta}{m} \cdot \sum_{e\in\mathcal{E}_{\rm tr}} (1 + 2\lambda C^e_{\text{IRMv1}}(t)) \frac{1}{n_e} \sum_{i=1}^{n_e} \ell'_i(t) \mathrm{Rad}(\alpha)_i \right| \\
&+ \left| \frac{\eta\lambda}{m} \cdot \sum_{e\in\mathcal{E}_{\rm tr}} 2C^e_{\text{IRMv1}} \frac{1}{n_e} \sum_{i=1}^{n_e} \ell''_i \hat{y}^e_i \cdot y^e_i \mathrm{Rad}(\alpha)_i \right| \\
&\le |\gamma_{j,r,1}(t)| + C\frac{\eta\lambda}{m} \|\mathbf{c}(t)\|_2.
\end{aligned}$$

Similarly, we have,

$$|\gamma_{j,r,2}(t+1)| \le |\gamma_{j,r,2}(t)| + C\frac{\eta\lambda}{m} \|\mathbf{c}(t)\|_2.$$

Taking the convergence time $T = \Omega\left(\frac{\log(\sigma_0/\epsilon)}{\eta\lambda\lambda_0}\right)$ we have that:

$$\|\mathbf{c}(T)\|_2 \le \epsilon.$$

Besides, at the time step T, the feature learning satisfies that:

$$\gamma_{j,r,1}(T) \le C\frac{\eta\lambda T}{m} \|\mathbf{c}(0)\|_2; \quad \gamma_{j,r,1}(T) \le C\frac{\eta\lambda T}{m} \|\mathbf{c}(0)\|_2.$$

To make sure that $\gamma_{j,r1,1}(T) = o_d(1)$ and $\gamma_{j,r1,2}(T) = o_d(1)$, we need the following condition:

$$C\frac{\eta\lambda T}{m} \|\mathbf{c}(0)\|_2 \le d^{-\frac{1}{2}},$$

which results in $\sigma_0 \le \frac{m\lambda_0}{d^{-1/2}\log(1/\epsilon)}$. Furthermore, we have that:

$$|f(\mathbf{x}_i, T)| \le \gamma_{j,r,1}(T) + \gamma_{j,r,2}(T) \le \gamma.$$

Combined with the condition that $C\frac{2\gamma}{m} < \lambda_0$, we obtain that:

$$\sigma_0 \le \frac{\lambda_0^2 m^2}{\log(1/\epsilon)}.$$

□

D.4. Proof for Proposition 3.3

Proposition D.7 (Restatement of Proposition 3.3)**.** *Consider training the CNN model with the same data as Theorem 3.1, suppose that* $\gamma_{j,r,1}(t_1) = \gamma_{j,r,1}(t_1-1)$ *and* $\gamma_{j,r,2}(t_1) = \gamma_{j,r,2}(t_1-1)$ *at the end of ERM pre-train* t_1 *and* $\mathcal{E}_{tr} = \{(0.25, 0.1), (0.25, 0.2)\}$*. Suppose that* $\delta > 0$*, and* $n > C\log(1/\delta)$*, with* C *being a positive constant, then with a high probability at least* $1-\delta$*, we have*

- $\sum_e C^e_{\mathit{IRMv1}}(t_1) = 0$.
- $\gamma_{j,r,1}(t_1+1) > \gamma_{j,r,1}(t_1)$.
- $\gamma_{j,r,2}(t_1+1) < \gamma_{j,r,2}(t_1)$.

Proof of Proposition D.7. According to the gradient descent for IRMV1 objective function, the evolution of coefficients can be expressed as:

$$\begin{aligned}\gamma_{j,r,1}(t+1) = \gamma_{j,r,1}(t) - \frac{\eta}{m} \cdot \sum_{e\in\mathcal{E}_{\mathrm{tr}}} (1 + 2\lambda C^e_{\mathrm{IRMv1}}(t))\frac{1}{n_e}\sum_{i=1}^{n_e} \ell'_i(t)\mathrm{Rad}(\alpha)_i \\ - \frac{\eta\lambda}{m} \cdot \sum_{e\in\mathcal{E}_{\mathrm{tr}}} 2C^e_{\mathrm{IRMv1}}\frac{1}{n_e}\sum_{i=1}^{n_e} \ell''_i \hat{y}^e_i \cdot y^e_i \mathrm{Rad}(\alpha)_i, \\ \gamma_{j,r,2}(t+1) = \gamma_{j,r,2}(t) - \frac{\eta}{m} \cdot \sum_{e\in\mathcal{E}_{\mathrm{tr}}} (1 + 2\lambda C^e_{\mathrm{IRMv1}}(t))\frac{1}{n_e}\sum_{i=1}^{n_e} \ell'_i(t)\mathrm{Rad}(\beta_e) \\ - \frac{\eta\lambda}{m} \cdot \sum_{e\in\mathcal{E}_{\mathrm{tr}}} 2C^e_{\mathrm{IRMv1}}\frac{1}{n_e}\sum_{i=1}^{n_e} \ell''_i \hat{y}^e_i \cdot y^e_i \mathrm{Rad}(\beta_e)_i,\end{aligned}$$

where $\ell''(y^e_i \cdot f(\mathbf{W}, \mathbf{x}^e_i)) = \frac{\exp(-y^e_i \cdot f(\mathbf{W},\mathbf{x}_i))}{(1+\exp(-y^e_i \cdot f(\mathbf{W},\mathbf{x}_i)))^2}$.

To simplify the notation, we further define

$$A^e_1 = \frac{1}{n_e}\sum_{i=1}^{n_e} \ell'_i \mathrm{Rad}(\alpha)_i$$

and

$$A^e_2 = \frac{1}{n_e}\sum_{i=1}^{n_e} \ell''_i \hat{y}^e_i y^e_i \mathrm{Rad}(\alpha)_i$$

. Similarly, we define

$$B^e_1 = \frac{1}{n_e}\sum_{i=1}^{n_e} \ell'_i \mathrm{Rad}(\beta_e)_i$$

and

$$B^e_2 = \frac{1}{n_e}\sum_{i=1}^{n_e} \ell''_i \hat{y}^e_i y^e_i \mathrm{Rad}(\beta_e)_i.$$

In the limit of $n \to \infty$, we have:

$$\begin{aligned}
\lim_{n\to\infty} A_1^1(t_1) &= -1/(1+e^{(\gamma_1+\gamma_2)})(1-\alpha)(1-\beta_1) - 1/(1+e^{\gamma_1-\gamma_2})(1-\alpha)\beta_1 \\
&\quad + 1/(1+e^{\gamma_2-\gamma_1})\alpha(1-\beta_1) + 1/(1+e^{-\gamma_1-\gamma_2})\alpha\beta_1, \\
\lim_{n\to\infty} A_1^2(t_1) &= -1/(1+e^{\gamma_1+\gamma_2})(1-\alpha)(1-\beta_2) - 1/(1+e^{\gamma_1-\gamma_2})(1-\alpha)\beta_2 \\
&\quad + 1/(1+e^{-\gamma_1+\gamma_2})\alpha(1-\beta_2) + 1/(1+e^{-\gamma_1-\gamma_2})\alpha\beta_2, \\
\lim_{n\to\infty} B_1^1(t_1) &= -1/(1+e^{\gamma_1+\gamma_2})(1-\alpha)(1-\beta_1) + 1/(1+e^{\gamma_1-\gamma_2})(1-\alpha)\beta_1 \\
&\quad - 1/(1+e^{-\gamma_1+\gamma_2})\alpha(1-\beta_1) + 1/(1+e^{-\gamma_1-\gamma_2})\alpha\beta_1, \\
\lim_{n\to\infty} B_1^2(t_1) &= -1/(1+e^{\gamma_1+\gamma_2})(1-\alpha)(1-\beta_2) + 1/(1+e^{\gamma_1-\gamma_2})(1-\alpha)\beta_2 \\
&\quad - 1/(1+e^{-\gamma_1+\gamma_2})\alpha(1-\beta_2) + 1/(1+e^{-\gamma_1-\gamma_2})\alpha\beta_2.
\end{aligned}$$

and,

$$\begin{aligned}
\lim_{n\to\infty} A_2^1(t_1) &= e^{\gamma_1+\gamma_2}/(1+e^{\gamma_1+\gamma_2})^2(1-\alpha)(1-\beta_1)(\gamma_1+\gamma_2) + e^{\gamma_1-\gamma_2}/(1+e^{\gamma_1-\gamma_2})^2(1-\alpha)\beta_1(\gamma_1-\gamma_2) \\
&\quad + e^{-\gamma_1+\gamma_2}/(1+e^{-\gamma_1+\gamma_2})^2\alpha(1-\beta_1)(\gamma_1-\gamma_2) + e^{-\gamma_1-\gamma_2}/(1+e^{-\gamma_1-\gamma_2})^2\alpha\beta_1(\gamma_1+\gamma_2), \\
\lim_{n\to\infty} A_2^2(t_1) &= e^{\gamma_1+\gamma_2}/(1+e^{\gamma_1+\gamma_2})^2(1-\alpha)(1-\beta_2)(\gamma_1+\gamma_2) + e^{\gamma_1-\gamma_2}/(1+e^{\gamma_1-\gamma_2})^2(1-\alpha)\beta_2(\gamma_1-\gamma_2) \\
&\quad + e^{-\gamma_1+\gamma_2}/(1+e^{-\gamma_1+\gamma_2})^2\alpha(1-\beta_2)(\gamma_1-\gamma_2) + e^{-\gamma_1-\gamma_2}/(1+e^{-\gamma_1-\gamma_2})^2\alpha\beta_2(\gamma_1+\gamma_2), \\
\lim_{n\to\infty} B_2^1(t_1) &= e^{\gamma_1+\gamma_2}/(1+e^{\gamma_1+\gamma_2})^2(1-\alpha)(1-\beta_1)(\gamma_1+\gamma_2) + e^{\gamma_1-\gamma_2}/(1+e^{\gamma_1-\gamma_2})^2(1-\alpha)\beta_1(-\gamma_1+\gamma_2) \\
&\quad + e^{-\gamma_1+\gamma_2}/(1+e^{-\gamma_1+\gamma_2})^2\alpha(1-\beta_1)(-\gamma_1+\gamma_2) + e^{-\gamma_1-\gamma_2}/(1+e^{-\gamma_1-\gamma_2})^2\alpha\beta_1(\gamma_1+\gamma_2), \\
\lim_{n\to\infty} B_2^2(t_1) &= e^{\gamma_1+\gamma_2}/(1+e^{\gamma_1+\gamma_2})^2(1-\alpha)(1-\beta_2)(\gamma_1+\gamma_2) + e^{\gamma_1-\gamma_2}/(1+e^{\gamma_1-\gamma_2})^2(1-\alpha)\beta_2(-\gamma_1+\gamma_2) \\
&\quad + e^{-\gamma_1+\gamma_2}/(1+e^{-\gamma_1+\gamma_2})^2\alpha(1-\beta_2)(-\gamma_1+\gamma_2) + e^{-\gamma_1-\gamma_2}/(1+e^{-\gamma_1-\gamma_2})^2\alpha\beta_2(\gamma_1+\gamma_2).
\end{aligned}$$

Because $\mathrm{Rad}(\alpha)_i$ and $\mathrm{Rad}(\beta)_i$ are random variables, applying Hoeffding's inequality, we have with probability at least $1-\delta$,

$$\left|A_1^1(t_1) - \lim_{n\to\infty} A_1^1(t_1)\right| \le \sqrt{\frac{4\log(1/\delta)}{n}}.$$

Similarly, we can apply concentration bound to other quantities and obtain the same bound.

By the assumption that $\gamma_{j,r,1}(t_1) = \gamma_{j,r,1}(t_1-1)$ and $\gamma_{j,r,2}(t_1) = \gamma_{j,r,2}(t_1-1)$, we have that $\sum_e A_1^e(t_1) = \sum_e B_1^e(t_1) = 0$:

$$\begin{aligned}
\lim_{n\to\infty}(A_1^1(t_1) + A_1^2(t_1)) &= -1/(1+e^{\gamma_1+\gamma_2})(1-\alpha)(2-\beta_1-\beta_2) - 1/(1+e^{\gamma_1-\gamma_2})(1-\alpha)(\beta_1+\beta_2) \\
&\quad + 1/(1+e^{-\gamma_1+\gamma_2})\alpha(2-\beta_1-\beta_2) + 1/(1+e^{-\gamma_1-\gamma_2})\alpha(\beta_1+\beta_2) = 0 \\
\lim_{n\to\infty}(B_1^1(t_1) + B_1^2(t_1)) &= -1/(1+e^{\gamma_1+\gamma_2})(1-\alpha)(2-\beta_1-\beta_2) + 1/(1+e^{\gamma_1-\gamma_2})(1-\alpha)(\beta_1+\beta_2) \\
&\quad + 1/(1+e^{-\gamma_1+\gamma_2})\alpha(2-\beta_1-\beta_2) + 1/(1+e^{-\gamma_1-\gamma_2})\alpha(\beta_1+\beta_2) = 0
\end{aligned}$$

Solving the above equations, we have,

$$\gamma_1^\infty(t_1) = \frac{1}{2}\log(G_m G_b) \quad \gamma_2^\infty(t_1) = \frac{1}{2}\log(G_m/G_b)$$

where we denote $\gamma_1^\infty(t_1) \triangleq \lim_{n\to\infty}\gamma_1(t_1)$ and $\gamma_2^\infty(t_1) \triangleq \lim_{n\to\infty}\gamma_1(t_2)$, $G_m = ((1-A)+\sqrt{(A-1)^2+4A})/(2A)$ and $G_b = ((1-B)+\sqrt{(B-1)^2+4B})/(2B)$, with $A = \alpha(\beta_1+\beta_2)/((1-\alpha)(2-\beta_1-\beta_2))$ and $B = \alpha(2-\beta_1-\beta_2)/((1-\alpha)*(\beta_1+\beta_2))$.

By the convexity of function $f(x) = e^x$, with a constant C, we have:

$$|\gamma_1 - \gamma_1^\infty| < \left|e^{\gamma_1} - e^{\gamma_1^\infty}\right| \le C\left|1/(1+e^{\gamma_1}) - 1/(1+e^{\gamma_1^\infty})\right| \le \sqrt{\frac{4\log(1/\delta)}{n}},$$
$$|\gamma_2 - \gamma_2^\infty| < \left|e^{\gamma_2} - e^{\gamma_2^\infty}\right| \le C\left|1/(1+e^{\gamma_2}) - 1/(1+e^{\gamma_2^\infty})\right| \le \sqrt{\frac{4\log(1/\delta)}{n}}.$$

Then we know that,

$$C^1_{\text{IRMv1}} = \frac{1}{n_1}\sum_{i=1}^{n_1} \ell_i' \hat{y}_i^1 y_i^1 = \gamma_1 A_1^1 + \gamma_2 B_1^1$$
$$C^2_{\text{IRMv1}} = \frac{1}{n_2}\sum_{i=1}^{n_2} \ell_i' \hat{y}_i^2 y_i^2 = \gamma_1 A_1^2 + \gamma_2 B_1^2$$

Therefore, we have that:

$$C^1_{\text{IRMv1}} + C^2_{\text{IRMv1}} = 0$$

Then the evolution of coefficients reduces to

$$\gamma_{j,r,1}(t+1) = \gamma_{j,r,1}(t) - \frac{\eta}{m}\cdot\sum_{e\in\mathcal{E}_{\text{tr}}}(1+2\lambda C^e_{\text{IRMv1}}(t))A_1^e(t) - \frac{\eta\lambda}{m}\cdot\sum_{e\in\mathcal{E}_{\text{tr}}} 2C^e_{\text{IRMv1}}A_2^e(t)$$
$$\gamma_{j,r,2}(t+1) = \gamma_{j,r,2}(t) - \frac{\eta}{m}\cdot\sum_{e\in\mathcal{E}_{\text{tr}}}(1+2\lambda C^e_{\text{IRMv1}}(t))B_1^e(t) - \frac{\eta\lambda}{m}\cdot\sum_{e\in\mathcal{E}_{\text{tr}}} 2C^e_{\text{IRMv1}}B_2^e(t)$$

Taking the solution of $\gamma_{j,r,1}(t_1)$, $\gamma_{j,r,2}(t_1)$ and value of α, β_1, β_2, we arrive at the conclusion that with a high a probability at least $1-\delta$ and $n > C_1\log(1/\delta)$ with C_1 being a positive constant, we have:

$$\gamma_{j,r,1}(t_1+1) > \gamma_{j,r,1}(t_1),$$
$$\gamma_{j,r,2}(t_1+1) < \gamma_{j,r,2}(t_1).$$

□

D.5. Proof for Corollary 3.4

Corollary D.8 (Restatement of Corollary 3.4)**.** *Consider training the CNN model with the data generated from Def. 2.1, suppose that $\gamma_{j,r,1}(t_1) = o(1)$ and $\gamma_{j,r,2}(t_1) = \Theta(1)$ at the end of ERM pre-train t_1 and $\mathcal{E}_{tr} = \{(0.25, 0.1), (0.25, 0.2)\}$. Suppose that $\delta > 0$, and $n > C\log(1/\delta)$, with C being a positive constant, then with a high probability at least $1-\delta$, we have*

$$\gamma_{j,r,1}(t_1+1) < \gamma_{j,r,1}(t_1).$$

Proof of Corollary D.8. Recall that the feature learning update rule:

$$\gamma_{j,r,1}(t+1) = \gamma_{j,r,1}(t) - \frac{\eta}{m}\cdot\sum_{e\in\mathcal{E}_{\text{tr}}}(1+2\lambda C^e_{\text{IRMv1}}(t))\frac{1}{n_e}\sum_{i=1}^{n_e}\ell_i'(t)\text{Rad}(\alpha)_i$$
$$- \frac{\eta\lambda}{m}\cdot\sum_{e\in\mathcal{E}_{\text{tr}}} 2C^e_{\text{IRMv1}}\frac{1}{n_e}\sum_{i=1}^{n_e}\ell_i''\hat{y}_i^e\cdot y_i^e\text{Rad}(\alpha)_i,$$
$$\gamma_{j,r,2}(t+1) = \gamma_{j,r,2}(t) - \frac{\eta}{m}\cdot\sum_{e\in\mathcal{E}_{\text{tr}}}(1+2\lambda C^e_{\text{IRMv1}}(t))\frac{1}{n_e}\sum_{i=1}^{n_e}\ell_i'(t)\text{Rad}(\beta_e)$$
$$- \frac{\eta\lambda}{m}\cdot\sum_{e\in\mathcal{E}_{\text{tr}}} 2C^e_{\text{IRMv1}}\frac{1}{n_e}\sum_{i=1}^{n_e}\ell_i''\hat{y}_i^e\cdot y_i^e\text{Rad}(\beta_e)_i,$$

Taking the value of $\gamma_{j,r,1}(t_1)$, $\gamma_{j,r,2}(t_1)$ and, we can conclude that:

$$\begin{aligned}
\lim_{n\to\infty} A_1^1(t_1) &= -1/(1+e^{\gamma_2})(1-\alpha)(1-\beta_1) - 1/(1+e^{-\gamma_2})(1-\alpha)\beta_1 + \\
&\quad 1/(1+e^{\gamma_2})\alpha(1-\beta_1) + 1/(1+e^{-\gamma_2})\alpha\beta_1 \\
&= 1/(1+e^{\gamma_2})(2\alpha-1)(1-\beta_1) + 1/(1+e^{-\gamma_2})(2\alpha-1)(\beta_1) \\
&= (2\alpha-1)[1/(1+e^{\gamma_2})(1-\beta_2) + 1/(1+e^{-\gamma_2})\beta_1)] \\
\lim_{n\to\infty} A_1^2(t_1) &= 1/(1+e^{\gamma_2})(2\alpha-1)(1-\beta_2) + 1/(1+e^{-\gamma_2})(2\alpha-1)(\beta_2) \\
&= (2\alpha-1)[1/(1+e^{\gamma_2})(1-\beta_2) + 1/(1+e^{-\gamma_2})\beta_2)] \\
\lim_{n\to\infty} B_1^1(t_1) &= -1/(1+e^{\gamma_2})(1-\alpha)(1-\beta_1) + 1/(1+e^{-\gamma_2})(1-\alpha)\beta_1 - \\
&\quad 1/(1+e^{\gamma_2})\alpha(1-\beta_1) + 1/(1+e^{-\gamma_2})\alpha\beta_1 \\
&= -1/(1+e^{\gamma_2})(1-\beta_1) + 1/(1+e^{-\gamma_2})\beta_1 \\
\lim_{n\to\infty} B_1^2(t_1) &= -1/(1+e^{\gamma_2})(1-\alpha)(1-\beta_2) + 1/(1+e^{-\gamma_2})(1-\alpha)\beta_2 - \\
&\quad 1/(1+e^{\gamma_2})\alpha(1-\beta_2) + 1/(1+e^{-\gamma_2})\alpha\beta_2 \\
&= -1/(1+e^{\gamma_2})(1-\beta_2) + 1/(1+e^{-\gamma_2})\beta_2
\end{aligned}$$

On the other hand,

$$\begin{aligned}
\lim_{n\to\infty} A_2^1(t_1) &= e^{\gamma_2}/(1+e^{\gamma_2})^2(1-\alpha)(1-\beta_1)(\gamma_2) + e^{-\gamma_2}/(1+e^{-\gamma_2})^2(1-\alpha)\beta_1(-\gamma_2) \\
&\quad + e^{+\gamma_2}/(1+e^{\gamma_2})^2\alpha(1-\beta_1)(-\gamma_2) + e^{-\gamma_2}/(1+e^{-\gamma_2})^2\alpha\beta_1(\gamma_2) \\
&= e^{\gamma_2}/(1+e^{\gamma_2})^2(1-2\alpha)(1-\beta_1) + e^{-\gamma_2}/(1+e^{-\gamma_2})^2(2\alpha-1)\beta_1\gamma_2 \\
\lim_{n\to\infty} A_2^2(t_1) &= e^{\gamma_2}/(1+e^{\gamma_2})^2(1-\alpha)(1-\beta_2)(\gamma_2) + e^{-\gamma_2}/(1+e^{-\gamma_2})^2(1-\alpha)\beta_2(-\gamma_2) \\
&\quad + e^{\gamma_2}/(1+e^{\gamma_2})^2\alpha(1-\beta_2)(-\gamma_2) + e^{-\gamma_2}/(1+e^{-\gamma_2})^2\alpha\beta_2(\gamma_2) \\
&= e^{\gamma_2}/(1+e^{\gamma_2})^2(1-2\alpha)(1-\beta_2) + e^{-\gamma_2}/(1+e^{-\gamma_2})^2(2\alpha-1)\beta_2\gamma_2 \\
\lim_{n\to\infty} B_2^1(t_1) &= e^{\gamma_2}/(1+e^{\gamma_2})^2(1-\alpha)(1-\beta_1)(\gamma_2) + e^{-\gamma_2}/(1+e^{-\gamma_2})^2(1-\alpha)\beta_1(\gamma_2) \\
&\quad + e^{\gamma_2}/(1+e^{\gamma_2})^2\alpha(1-\beta_1)(\gamma_2) + e^{-\gamma_2}/(1+e^{-\gamma_2})^2\alpha\beta_1(\gamma_2), \\
\lim_{n\to\infty} B_2^2(t_1) &= e^{\gamma_2}/(1+e^{\gamma_2})^2(1-\alpha)(1-\beta_2)(\gamma_2) + e^{-\gamma_2}/(1+e^{-\gamma_2})^2(1-\alpha)\beta_2(\gamma_2) \\
&\quad + e^{\gamma_2}/(1+e^{\gamma_2})^2\alpha(1-\beta_2)(\gamma_2) + e^{-\gamma_2}/(1+e^{-\gamma_2})^2\alpha\beta_2(\gamma_2).
\end{aligned}$$

Finally, taking the value of environment of $(\alpha, \beta_1, \beta_2) = (0.25, 0.1, 0.2)$, we conclude that with a high a probability at least $1-\delta$ and $n > C_1 \log(1/\delta)$ with C_1 being a positive constant, we have:

$$\gamma_{j,r,1}(t_1+1) < \gamma_{j,r,1}(t_1).$$

□

Algorithm 1 FAT: **F**eature **A**ugmented **T**raining

Input: Training data $\mathcal{D}_{\mathrm{tr}}$; the maximum augmentation rounds K; predictor $f := w \circ \varphi$; length of inner training epochs t; termination threshold p;
Initialize groups $G^a \leftarrow \mathcal{D}_{\mathrm{tr}}, G^r \leftarrow \{\}$;
for $k \in [1, \ldots, K]$ **do**
  Randomly initialize w_k;
  for $j \in [1, \ldots, t]$ **do**
    Obtain ℓ_{FAT} with G via Eq. 24;
    Update w_k, φ with ℓ_{FAT};
  end for
  `// Early Stop if` $f_k = w_k \circ \varphi$ `fails to find new features.`
  if Training accuracy of f_k is smaller than p **then**
    Set $K = k - 1$ and terminate the loop;
  end if
  Split $\mathcal{D}_{\mathrm{tr}}$ into groups $\mathcal{D}^a_k, \mathcal{D}^r_k$ according to whether f_k classifies the examples in $\mathcal{D}_{\mathrm{tr}}$ correctly or not;
  Update groups $G^a \leftarrow G^a \cup \{\mathcal{D}^a_k\}, G^r \leftarrow G^r \cup \{\mathcal{D}^r_k\}$;
end for
Synthesize the final classifier $w \leftarrow \frac{1}{K}\sum_{i=1}^{K} w_i$;
return $f = w \circ \varphi$;

E. Feature Augmentated Training

E.1. Rich Features for OOD Generalization

The results in Sec. 3 imply the necessity of learning all potentially useful features during the pre-training stage for OOD generalization. Otherwise, the OOD training is less likely to enhance the poorly learned features. It also explains the success of learning diverse and rich features by weight averaging (Rame et al., 2022; Arpit et al., 2022) and rich feature construction (or Bonsai) (Zhang et al., 2022), and other approaches (Ye et al., 2022; Ramé et al., 2022).

Despite the empirical success, however, the learning of rich features in both Bonsai and weight averaging is unstable and expensive. On the one hand, they may discard previously learned useful features or fail to explore all the desired features as it is hard to evaluate the quality of the intermediate learned features. On the other hand, they also need multiple initializations and training of the whole networks with different random seeds to encourage the diversity of feature learning, which brings more instability and computational overhead, especially when applied to large and deep networks.

E.2. The FAT Algorithm

To overcome the limitations of previous rich feature learning algorithms, we propose **F**eature **A**ugmented **T**raining (FAT), that directly augment the feature learning in an iterative manner.

Intuitively, the potentially useful features presented in the training data are features that have non-trivial correlations with labels, or using the respective feature to predict the labels is able to achieve a *non-trivial training performance*. Moreover, the invariance principle assumes that the training data comes from different environments (Arjovsky et al., 2019), which implies that each set of features can only dominate the correlations with labels in a *subset* of data. Therefore, it is possible to differentiate the distinct sets of useful features entangled in the training data into different subsets, where ERM can effectively learn the dominant features presented in the corresponding subset as shown in Theorem 3.1.

The intuition naturally motivates an iterative rich feature learning algorithm, i.e., FAT, that identifies the subsets containing distinct features and explores to learn new features in multiple rounds. The details of FAT are given in Algorithm 1, where we are given a randomly initialized or pre-trained model $f = w \circ \varphi$ that consists of a featurizer φ and a classifier w. In round k, FAT first identifies the subset that contains the already learned features by collecting the samples where f yields the correct prediction, denoted as G^r_k, and the subset of samples that contains the features that have not been learned, denoted as G^a_k.

At the k-th round, given the grouped subsets $G = \{G^r, G^a\}$ with $2k - 1$ groups, where $G^a = \{\mathcal{D}^a_i\}_{i=0}^{k-1}$ is the grouped sets for new feature augmentation, and $G^r = \{\mathcal{D}^r_i\}_{i=1}^{k-1}$ is the grouped sets for already learned feature retention (notice that

$\mathcal{D}_0^r$ is the empty set), FAT performs distributionally robust optimization (DRO) (Namkoong and Duchi, 2016; Zhang et al., 2022) on G^a to explore new features that have not been learned in previous rounds. Meanwhile, FAT also needs to *retain* the already learned features by minimizing the empirical risk at G^r. Then, the FAT objective at round k is

$$\ell_{\text{FAT}} = \max_{\mathcal{D}_i^a \in G^a} \ell_{\mathcal{D}_i^a}(w_k \circ \varphi) + \lambda \cdot \sum_{\mathcal{D}_i^r \in G^r} \ell_{\mathcal{D}_i^r}(w_i \circ \varphi), \tag{24}$$

where $\ell_{\mathcal{D}_i}(w \circ \varphi)$ refers to the empirical risk of $w \circ \varphi$ evaluated at the subset $\mathcal{D}_i$, and $\{w_i | 1 \leq i \leq k-1\}$ are the historical classifiers trained in round i.

Relations with previous rich feature learning algorithms. Compared with previous rich feature learning algorithms, FAT *directly* trades off the exploration of new features and the retention of the already learned features. Although Bonsai also adopts DRO to explore new features, the isolation of new feature exploration and already learned feature synthesis makes the feature learning in Bonsai more unstable. In other words, Bonsai can not evaluate the intermediate feature learning results due to the *indirect* feature exploration and synthesis. Consequently, Bonsai can not control when to stop the new feature exploration, and thus may fail to explore all of the desired features or discard important features. Besides, the multiple re-initializations and re-training of the whole network in Bonsai could also lead to suboptimal performance and meanwhile require more computational overhead.

Practical implementations. Algorithm 1 requires to store $2K-1$ subsets and a larger memory cost in training the network, which may cause additional storage burden when φ contains a massive amount of parameters (Koh et al., 2021). Hence, we propose a lightweight variant of FAT (denoted as iFAT) which only retains the latest subsets and historical classifiers. Throughout the whole experiments, we will use iFAT and find that iFAT already achieves state-of-the-art. More details are given in Appendix F.

As iFAT stores only the latest augmentation and retention subsets, inspecting the training performance for termination check (line 10 of Algorithm 1) may not be suitable. However, one can still inspect the performance in either an OOD validation set to check the quality of the intermediate feature representations, or the retention set to check whether learning new features leads to a severe contradiction of the already learned features (FAT should terminate if so).

F. More Details about iFAT

As mentioned in Sec. E.2 that, when the featurizer is implemented as a deep net that have a massive amount of parameters, backpropagating through Algorithm 1 can allocate too much memory for propagating with $2K-1$ batches of data. It is common for many realistic benchmarks such as Camelyon17 and FMoW in wilds benchmark (Koh et al., 2021) that adopts a DenseNet (Huang et al., 2017) with 121 layers as the featurizer. To relieve the exceeding computational and memory overhead, we propose a lightweight version of FAT, denoted as FAT. Instead of storing all of historical subsets and classifiers, iFAT iteratively use the augmentation and retention sets and historical classifier from only the last round. In contrast, previous rich feature learning algorithm (Zhang et al., 2022; Rame et al., 2022) incurs a high computational and memory overhead as the round grows. For example, in RxRx1, we have to reduce the batch size of Bonsai to allow the proceeding of rounds ≥ 3.

We elaborate the detailed algorithmic description of iFAT in Algorithm 2.

G. Empirical Study

We conduct extensive experiments on ColoredMNIST (Chen et al., 2022) and Wilds (Koh et al., 2021) to verify the effectiveness of FAT in learning richer features than ERM and the state-of-the-art algorithm Bonsai (Zhang et al., 2022).

Proof-of-concept study on ColoredMNIST. We first conduct a proof-of-concept study using ColoredMNIST (Chen et al., 2022) and examine the feature learning performance of FAT under various conditions. We consider both the original ColoredMNIST with $\mathcal{E}_{\text{tr}} = \{(0.25, 0.1), (0.25, 0.2)\}$ (denoted as ColoredMNIST-025), where spurious features are better correlated with labels, and the modified ColoredMNIST (denoted as ColoredMNIST-01) with $\mathcal{E}_{\text{tr}} = \{(0.1, 0.2), (0.1, 0.25)\}$, where invariant features are better correlated with labels. We compare the OOD performance of the features learned by FAT, with that of ERM and the state-of-the-art rich feature learning algorithm Bonsai (Zhang et al., 2022). Based on the features learned by ERM, Bonsai, and FAT, we adopt various state-of-the-art OOD objectives including IRMv1 (Arjovsky et al., 2019), VREx (Krueger et al., 2021), IRMX (Chen et al., 2022), IB-IRM (Ahuja et al.,

Algorithm 2 FAT: **F**eature **A**ugmented **T**raining

Input: Training data $\mathcal{D}_{\rm tr}$; the maximum augmentation rounds K; predictor $f := w \circ \varphi$; length of inner training epochs e; termination threshold p;
Initialize groups $G^a \leftarrow \mathcal{D}_{\rm tr}, G^r \leftarrow \{\}$;
for $k \in [1, \ldots, K]$ **do**
  Randomly initialize w_k;
  for $j \in [1, \ldots, e]$ **do**
    Obtain ℓ_{FAT} with G via Eq. 24;
    Update w_k, φ with ℓ_{FAT};
  end for
  // Early Stop if $f_k = w_k \circ \varphi$ fails to find new features.
  if Training accuracy of f_k is smaller than p **then**
    Set $K = k - 1$ and terminate the loop;
  end if
  if $k > 1$ **then**
    // Hence it doesnot need to maintain all historical classifiers.
    Update $w_k \leftarrow (w_{k-1}, w_k)$;
  end if
  Split $\mathcal{D}_{\rm tr}$ into groups $\mathcal{D}_k^a, \mathcal{D}_k^r$ according to f_k;
  // Hence it doesnot need to maintain all historical subsets.
  Update groups $G^a \leftarrow \{\mathcal{D}_k^a\}, G^r \leftarrow \{\mathcal{D}_k^r\}$;
end for
return $f = w \circ \varphi$;

Table 1. OOD performance on COLOREDMNIST datasets initialized with different representations.

	COLOREDMNIST-025				COLOREDMNIST-01			
	ERM-NF	ERM	BONSAI	FAT	ERM-NF	ERM	BONSAI	FAT
ERM	17.14 (±0.73)	12.40 (±0.32)	11.21 (±0.49)	**17.27** (±2.55)	73.06 (±0.71)	73.75 (±0.49)	70.95 (±0.93)	**76.05** (±1.45)
IRMV1	67.29 (±0.99)	59.81 (±4.46)	70.28 (±0.72)	**70.57** (±0.68)	76.89 (±3.25)	73.84 (±0.56)	76.71 (±4.10)	**82.33** (±1.77)
V-REX	68.62 (±0.73)	65.96 (±1.29)	70.31 (±0.66)	**70.82** (±0.59)	83.52 (±2.52)	81.20 (±3.27)	82.61 (±1.76)	**84.70** (±0.69)
IRMX	67.00 (±1.95)	64.05 (±0.88)	70.46 (±0.42)	**70.78** (±0.61)	81.61 (±1.98)	75.97 (±0.88)	80.28 (±1.62)	**84.34** (±0.97)
IB-IRM	56.09 (±2.04)	59.81 (±4.46)	70.28 (±0.72)	**70.57** (±0.68)	75.81 (±0.63)	73.84 (±0.56)	76.71 (±4.10)	**82.33** (±1.77)
CLOVE	58.67 (±7.69)	65.78 (±0.00)	65.57 (±3.02)	**65.78** (±2.68)	75.66 (±10.6)	74.73 (±0.36)	72.73 (±1.18)	**75.12** (±1.08)
IGA	51.22 (±3.67)	62.43 (±3.06)	**70.17** (±0.89)	67.11 (±3.40)	74.20 (±2.45)	73.74 (±0.48)	74.72 (±3.60)	**83.46** (±2.17)
FISHR	69.38 (±0.39)	67.74 (±0.90)	68.75 (±1.10)	**70.56** (±0.97)	77.29 (±1.61)	82.23 (±1.35)	84.19 (±0.66)	**84.26** (±0.93)
ORACLE	71.97 (±0.34)				86.55 (±0.27)			

2021), CLOvE (Wald et al., 2021), IGA (Koyama and Yamaguchi, 2020) and Fishr (Rame et al., 2021) for OOD training, in order to evaluate the practical quality of the learned features. The feature representations are frozen once initialized for the OOD training as fine-tuning the featurizer can distort the pre-trained features (Kumar et al., 2022b). We also compare FAT with the common training approach that uses unfrozen ERM features, denoted as ERM-NF. For Bonsai, we trained 2 rounds following Zhang et al. (2022), while for FAT the automatic termination stopped at round 2 in COLOREDMNIST-025 and round 3 in COLOREDMNIST-01. For ERM, we pre-trained the model with the same number of overall epochs as FAT in COLOREDMNIST-01, while early stopping at the number of epochs of 1 round in COLOREDMNIST-025 to prevent over-fitting. All methods adopted the same backbone and the same training protocol following previous works (Zhang et al., 2022; Chen et al., 2022). More details are given in Appendix H.1.

The results are reported in Table 1. It can be found that ERM will learn insufficiently good features under both stronger spurious correlations and invariant correlations, confirming our discussion in Sec. 3. Besides, Bonsai learns richer features in COLOREDMNIST-025 and boosts OOD performance, but Bonsai sometimes leads to suboptimal performances in COLOREDMNIST-01, which could be caused by the unstable feature learning in Bonsai. In contrast, FAT consistently improves the OOD performance of all OOD objectives for all the COLOREDMNIST datasets, demonstrating the advances of direct feature learning control in FAT than Bonsai and ERM.

Experiments on real-world benchmarks. We also compare FAT with ERM and Bonsai in 6 real-world OOD generalization

Table 2. OOD generalization performances on WILDS benchmark.

INIT.	METHOD	CAMELYON17	CIVILCOMMENTS	FMOW	IWILDCAM	AMAZON	RXRX1
		Avg. acc. (%)	Worst acc. (%)	Worst acc. (%)	Macro F1	10-th per. acc. (%)	Avg. acc. (%)
ERM	DFR†	95.14 (±1.96)	**77.34** (±0.50)	41.96 (±1.90)	23.15 (±0.24)	48.00 (±0.00)	-
ERM	DFR-s†	-	82.24 (±0.13)	56.17 (±0.62)	52.44 (±0.34)	-	-
Bonsai	DFR†	95.17 (±0.18)	77.07 (±0.85)	43.26 (±0.82)	21.36 (±0.41)	46.67 (±0.00)	-
Bonsai	DFR-s†	-	81.26 (±1.86)	58.58 (±1.17)	50.85 (±0.18)	-	-
FAT	DFR†	**95.28** (±0.19)	**77.34** (±0.59)	**43.54** (±1.26)	**23.54** (±0.52)	**49.33** (±0.00)	-
FAT	DFR-s†	-	79.56 (±0.38)	57.69 (±0.78)	52.31 (±0.38)	-	-
ERM	ERM	74.30 (±5.96)	55.53 (±1.78)	33.58 (±1.02)	28.22 (±0.78)	51.11 (±0.63)	30.21 (±0.09)
ERM	GroupDRO	76.09 (±6.46)	69.50 (±0.15)	33.03 (±0.52)	28.51 (±0.58)	52.00 (±0.00)	29.99 (±0.13)
ERM	IRMv1	75.68 (±7.41)	68.84 (±0.95)	33.45 (±1.07)	28.76 (±0.45)	52.00 (±0.00)	30.10 (±0.05)
ERM	V-REx	71.60 (±7.88)	69.03 (±1.08)	33.06 (±0.46)	28.82 (±0.47)	52.44 (±0.63)	29.88 (±0.35)
ERM	IRMX	73.49 (±9.33)	68.91 (±1.19)	33.13 (±0.86)	28.82 (±0.47)	52.00 (±0.00)	30.10 (±0.05)
Bonsai	ERM	73.98 (±5.30)	63.34 (±3.49)	31.91 (±0.51)	28.27 (±1.05)	48.58 (±0.56)	24.22 (±0.44)
Bonsai	GroupDRO	72.82 (±5.37)	70.23 (±1.33)	33.12 (±1.20)	27.16 (±1.18)	42.67 (±1.09)	22.95 (±0.46)
Bonsai	IRMv1	73.59 (±6.16)	68.39 (±2.01)	32.51 (±1.23)	27.60 (±1.57)	47.11 (±0.63)	23.35 (±0.43)
Bonsai	V-REx	76.39 (±5.32)	68.67 (±1.29)	33.17 (±1.26)	25.81 (±0.42)	48.00 (±0.00)	23.34 (±0.42)
Bonsai	IRMX	64.77 (±10.1)	69.56 (±0.95)	32.63 (±0.75)	27.62 (±0.66)	46.67 (±0.00)	23.34 (±0.40)
FAT	ERM	77.80 (±2.48)	68.11 (±2.27)	33.13 (±0.78)	28.47 (±0.67)	**52.89** (±0.63)	**30.66** (±0.42)
FAT	GroupDRO	**80.41** (±3.30)	**71.29** (±0.46)	33.55 (±1.67)	28.38 (±1.32)	52.58 (±0.56)	29.99 (±0.11)
FAT	IRMv1	77.97 (±3.09)	70.33 (±1.14)	**34.04** (±0.70)	**29.66** (±1.52)	**52.89** (±0.63)	29.99 (±0.19)
FAT	V-REx	75.12 (±6.55)	70.97 (±1.06)	34.00 (±0.71)	29.48 (±1.94)	**52.89** (±0.63)	30.57 (±0.53)
FAT	IRMX	76.91 (±6.76)	71.18 (±1.10)	33.99 (±0.73)	29.04 (±2.96)	**52.89** (±0.63)	29.92 (±0.16)

table†DFR/DFR-s use an additional OOD dataset to evaluate invariant and spurious feature learning, respectively.

datasets curated by Koh et al. (2021) that contain complicated features and distribution shifts. The learned features are evaluated with several representative state-of-the-art OOD objectives in WILDS, including GroupDro (Sagawa* et al., 2020), IRMv1 (Arjovsky et al., 2019), VREx (Krueger et al., 2021) as well as IRMX (Chen et al., 2022). By default, we train ERM, Bonsai and FAT the same number of steps, and kept the rounds of Bonsai and FAT the same (though Bonsai still requires one more round for feature synthesis). The only exception is in RXRX1 where both Bonsai and FAT required more steps than ERM to converge. We use the same evaluation protocol following the practice in the literature (Koh et al., 2021; Shi et al., 2022; Zhang et al., 2022; Chen et al., 2022) to ensure a fair comparison. More details are given in Appendix H.2.

In addition to OOD objectives, we evaluate the learned features with Deep Feature Reweighting (DFR) (Kirichenko et al., 2022). DFR uses an additional OOD validation set where the *spurious correlation does not hold*, to perform logistic regression based on the learned features. Intuitively, DFR can serve as a proper measure for the quality of learned invariant features (Izmailov et al., 2022). When the original dataset does not provide a proper OOD validation set, e.g., CAMELYON17, we use an alternative implementation based on a random split of the training and test data to perform the invariant feature quality measure (Rosenfeld et al., 2022). Similarly, we also report DFR-s by regression with the environment labels (when available) to evaluate the spurious feature learning of different methods. More details are given in Appendix H.2.2.

The results are presented in Table 2. Similarly, when the tasks grow more challenging and neural architectures become more complicated, the ERM learned features can have a lower quality as discussed Sec. 3. For example, ERM can not sufficiently learn all useful features in FMoW, while ERM can learn more spurious correlations in CivilComments. Moreover, it can also be observed the instability of Bonsai in learning richer features that Bonsai even underperforms ERM in rich feature learning and OOD generalization in multiple datasets. In contrast, FAT consistently achieves the best invariant feature learning performance across various challenging realistic datasets. Meanwhile, compared to ERM and Bonsai, FAT also reduces over-fitting to the spurious feature learning led by spurious correlations. As a result, FAT achieves consistent improvements when the learned features are applied to various OOD objectives.

The termination check in FAT. As elaborated in Sec. E.2, a key difference between FAT and previous rich feature learning algorithms such as Bonsai is that FAT is able

Table 3. Performances in various sets at different FAT rounds.

COLOREDMNIST-025	ROUND-1	ROUND-2	ROUND-3
TRAINING ACC.	85.08± 0.14	71.87± 0.96	84.93± 1.26
RETENTION ACC.	-	88.11± 4.28	43.82± 0.59
OOD ACC.	11.08± 0.30	70.64± 0.62	10.07± 0.26

to access the intermediate feature representations and thus can perform the automatic termination check and learn the desired features stably. To verify, we list the FAT performances in various subsets of COLOREDMNIST-025 at different rounds in Table 3. By inspecting the retention accuracy, after FAT learns sufficiently good features at Round 2, it is not necessary to proceed with Round 3 as it will destroy the already learned features and lead to degenerated retention and OOD performance. More details and results are given in Appendix H.1.

H. More Details about the Experiments

In this section, we provide more details and the implementation, evaluation and hyperparameter setups in complementary to the experiments in Sec. G.

H.1. More details about COLOREDMNIST experiments

Datasets. In the controlled experiments with COLOREDMNIST, we follow the evaluation settings as previous works (Arjovsky et al., 2019; Zhang et al., 2022; Chen et al., 2022). In addition to the original COLOREDMNIST with $\mathcal{E}_{\text{tr}} = \{(0.25, 0.1), (0.25, 0.2)\}$ (denoted as COLOREDMNIST-025) where spurious features are better correlated with labels, we also incorporate the modified one (denoted as COLOREDMNIST-01) with $\mathcal{E}_{\text{tr}} = \{(0.1, 0.2), (0.1, 0.25)\}$ where invariant features are better correlated with labels, since both cases can happen at real world.

Architecture and optimization. To ensure a fair comparison, we use 4-Layer MLP with a hidden dimension of 256 as the backbone model for all methods, where we take the first 3 layers as the featurizer and the last layer as the classifier, following the common practice (Gulrajani and Lopez-Paz, 2021; Koh et al., 2021). For the optimization of the models, we use the Adam (Kingma and Ba, 2015) optimizer with a learning rate of $1e-3$ and a weight decay of $1e-3$. We report the mean and standard deviation of the performances of different methods with each configuration of hyperparameters 10 times with the random seeds from 1 to 10.

Implementation of ERM-NF and OOD objectives. For the common pre-training protocol with ERM, our implementation follows the previous works (Zhang et al., 2022). Specifically, we first train the model with $\{0, 50, 100, 150, 200, 250\}$ epochs and then apply the OOD regularization of various objectives with a penalty weight of $\{1e1, 1e2, 1e3, 1e4, 1e5\}$. We adopt the implementations from Zhang et al. (2022) for various OOD objectives, including IRMv1 (Arjovsky et al., 2019),VREx (Krueger et al., 2021),IB-IRM (Ahuja et al., 2021),CLOvE (Wald et al., 2021),IGA (Koyama and Yamaguchi, 2020) and Fishr (Rame et al., 2021) Besides, we also incorporate the state-of-the-art OOD objective proposed by Chen et al. (2022) that is able to resolve both COLOREDMNIST-025 and COLOREDMNIST-01.

Evaluation of feature learning methods. For the sake of fairness in comparison, by default, we train all feature learning methods by the same number of epochs and rounds (if applicable). For the implementation Bonsai, we strictly follow the recommended setups provided by Zhang et al. (2022), [6] where we train the model with Bonsai by 2 rounds with 50 epochs for round 1, 500 epochs for round 2, and 500 epochs for the synthesize round in COLOREDMNIST-025. While in COLOREDMNIST-01, round 1 contains 150 epochs, round 2 contains 400 epochs and the synthesize round contains 500 epochs. For the implementation of FAT, we train the model with 2 rounds of FAT in COLOREDMNIST-025, and 3 rounds of FAT in COLOREDMNIST-01, where each round contains 150 epochs. While for the retain penalty, we find using a fixed number of 0.01 already achieved sufficiently good performance. ERM only contains 1 round, for which we train the model with 150 epochs in COLOREDMNIST-025 as we empirically find more epochs will incur severe performance degeneration in COLOREDMNIST-025. While in COLOREDMNIST-01, we train the model with ERM by 500 epochs to match up the overall training epochs of FAT and Bonsai. We provide a detailed distribution of the number of epochs in each round in Table 4. It can be found that, although Bonsai costs $2-3$ times of training epochs more than ERM and FAT, Bonsai does not necessarily find better feature representations for OOD training, as demonstrated in Table. 1. In contrast, FAT significantly and consistently learns richer features given both COLOREDMNIST-025 and COLOREDMNIST-01 than ERM, which shows the superiority of FAT.

[6] https://github.com/TjuJianyu/RFC

Table 4. Number of epochs in each round of various feature learning algorithms.

CMNIST-025	Round-1	Round-2	Round-3	Syn. Round
ERM	150	-	-	-
Bonsai	50	150	-	500
FAT	150	150	-	-
CMNIST-01	Round-1	Round-2	Round-3	Syn. Round
ERM	500	-	-	-
Bonsai	150	400	-	500
FAT	150	150	150	-

The termination check in FAT. A key difference between FAT and previous rich feature learning algorithms is that FAT is able to perform the automatic termination check and learn the desired features stably. As elaborated in Sec. E.2, FAT can terminate automatically by inspecting the retention accuracy. To verify, we list the FAT performances in various subsets of ColoredMNIST-025 and ColoredMNIST-01 at different rounds. We use a termination accuracy of 130%, which trades off the exploration (i.e., training accuracy as 80%) and the retention (i.e., retention accuracy as 50%) properly. As shown in Table 5, in ColoredMNIST-025 (ColoredMNIST-01), after FAT learns sufficiently good features at Round 2 (3), respectively, it is not necessary to proceed with Round 3 (4) as it will destroy the already learned features and lead to degenerated retention performance (i.e., the sum of training and retention accuracies is worse than 130%.

Table 5. Performances in various sets at different FAT rounds.

ColoredMNIST-025	Round-1	Round-2	Round-3	
Training Acc.	85.08± 0.14	71.87± 0.96	84.93± 1.26	
Retention Acc.	-	88.11± 4.28	43.82± 0.59	
OOD Acc.	11.08± 0.30	70.64± 0.62	10.07± 0.26	
ColoredMNIST-01	Round-1	Round-2	Round-3	Round-4
Training Acc.	88.63± 0.15	74.25± 1.23	86.07± 0.36	77.29± 0.24
Retention Acc.	-	85.91± 1.78	48.05± 1.39	29.09± 1.15
OOD Acc.	73.50± 0.41	17.32± 2.69	85.40± 0.54	12.48± 2.85

H.2. More details about Wilds experiments

In this section, we provide more details about the Wilds datasets used in the experiments as well as the evaluation setups.

H.2.1. Dataset description.

To evaluate the feature learning performance given data from realistic scenarios, we select 6 challenging datasets from Wilds (Koh et al., 2021) benchmark. The datasets contain various realistic distribution shifts, ranging from domain distribution shifts, subpopulation shifts and the their mixed. A summary of the basic information and statistics of the selected Wilds datasets can be found in Table. 6, Table. 7, respectively. In the following, we will give a brief introduction to each of the datasets. More details can be found in the Wilds paper (Koh et al., 2021).

Table 6. A summary of datasets information from Wilds.

Dataset	Data (x)	Class information	Domains	Metric	Architecture
Amazon	Product reviews	Star ratings (5 classes)	7,676 reviewers	10-eth percentile acc.	DistillBERT
Camelyon17	Tissue slides	Tumor (2 classes)	5 hospitals	Avg. acc.	DenseNet-121
CivilComments	Online comments	Toxicity (2 classes)	8 demographic groups	Wr. group acc.	DistillBERT
FMoW	Satellite images	Land use (62 classes)	16 years x 5 regions	Wr. group acc.	DenseNet-121
iWildCam	Photos	Animal species (186 classes)	324 locations	Macro F1	ResNet-50
RxRx1	Cell images	Genetic treatments (1,139 classes)	51 experimental batches	Avg. acc	ResNet-50

Amazon. We follow the Wilds splits and data processing pipeline for the Amazon dataset (Ni et al., 2019). It provides 1.4 million comments collected from $7,676$ Amazon customers. The task is to predict the score (1-5 stars) for each review. The domains d are defined according to the reviewer/customer who wrote the product reviews. The evaluation metric used for

Table 7. A summary of datasets statistics from WILDS.

Dataset	# Examples			# Domains		
	train	val	test	train	val	test
AMAZON	1,000,124	100,050	100,050	5,008	1,334	1,334
CAMELYON17	302,436	34,904	85,054	3	1	1
CIVILCOMMENTS	269,038	45,180	133,782	-	-	-
FMOW	76,863	19,915	22,108	11	3	2
IWILDCAM	129,809	14,961	42,791	243	32	48
RXRX1	40,612	9,854	34,432	33	4	14

the task is 10th percentile of per-user accuracies in the OOD test sets, and the backbone model is a DistilBert (Sanh et al., 2019), following the WILDS protocol (Koh et al., 2021).

Camelyon17. We follow the WILDS splits and data processing pipeline for the Camelyon17 dataset (Bándi et al., 2019). It provides $450,000$ lymph-node scans from 5 hospitals. The task in Camelyon17 is to take the input of 96×96 medical images to predict whether there exists a tumor tissue in the image. The domains d refers to the index of the hospital where the image was taken. The training data are sampled from the first 3 hospitals where the OOD validation and test data are sampled from the 4-th and 5-th hospital, respectively. We will use the average accuracy as the evaluation metric and a DenseNet-121 (Huang et al., 2017) as the backbone for the featurizer.

CivilComments. We follow the WILDS splits and data processing pipeline for the CivilComments dataset (Borkan et al., 2019). It provides $450,000$ comments collected from online articles. The task is to classify whether an online comment text is toxic or non-toxic. The domains d are defined according to the demographic features, including male, female, LGBTQ, Christian, Muslim, other religions, Black, and White. CivilComments is used to study the subpopulation shifts, here we will use the worst group/domain accuracy as the evaluation metric. As for the backbone of the featurizer, we will use a DistillBert (Sanh et al., 2019) following WILDS (Koh et al., 2021).

FMoW. We follow the WILDS splits and data processing pipeline for the FMoW dataset (Christie et al., 2018). It provides satellite images from 16 years and 5 regions. The task in FMoW is to classify the images into 62 classes of building or land use categories. The domain is split according to the year that the satellite image was collected, as well as the regions in the image which could be Africa, America, Asia, Europe or Oceania. Distribution shifts could happen across different years and regions. The training data contains data collected before 2013, while the validation data contains images collected within 2013 to 2015, and the test data contains images collected after 2015. The evaluation metric for FMoW is the worst region accuracy and the backbone model for the featurizer is a DenseNet-121 (Huang et al., 2017).

iWildCam. We follow the WILDS splits and data processing pipeline for the iWildCam dataset (Beery et al., 2020). It is consist of $203,029$ heat or motion-activated photos of animal specifies from 323 different camera traps across different countries around the world. The task of iWildCam is to classify the corresponding animal specifies in the photos. The domains is split according to the locations of the camera traps which could introduce the distribution shifts. We will use the Macro F1 as the evaluation metric and a ResNet-50 (He et al., 2016) as the backbone for the featurizer.

RxRx1. We follow the WILDS splits and data processing pipeline for the RxRx1 dataset (Taylor et al., 2019). The input is an image of cells taken by fluorescent microscopy. The cells can be genetically perturbed by siRNA and the task of RxRx1 is to predict the class of the corresponding siRNA that have treated the cells. There exists $1,139$ genetic treatments and the domain shifts are introduced by the experimental batches. We will use the average accuracy of the OOD experimental batches as the evaluation metric and a ResNet-50 (He et al., 2016) as the backbone for the featurizer.

H.2.2. TRAINING AND EVALUATION DETAILS.

We follow previous works to implement and evaluate different methods used in our experiments (Koh et al., 2021). The information of the referred paper and code is listed as in Table. 8.

The general hyperparemter setting inherit from the referred codes and papers, and are as listed in Table 9. We use the same backbone models to implement the featurizer (He et al., 2016; Huang et al., 2017; Sanh et al., 2019). By default, we repeat the experiments by 3 runs with the random seeds of $0, 1, 2$. While for Camelyon17, we follow the official guide to repeat 10 times with the random seeds from 0 to 9.

Table 8. The information of the referred paper and code.

Paper	Commit	Code
WILDS (Koh et al., 2021)	v2.0.0	https://wilds.stanford.edu/
Fish (Shi et al., 2022)	333efa24572d99da0a4107ab9cc4af93a915d2a9	https://github.com/YugeTen/fish
Bonsai (Zhang et al., 2022)	33b9ecad0ce8b3462793a2da7a9348d053c06ce0	https://github.com/TjuJianyu/RFC
DFR (Kirichenko et al., 2022; Izmailov et al., 2022)	6d098440c697a1175de6a24d7a46ddf91786804c	https://github.com/izmailovpavel/spurious_feature_learning

Table 9. General hyperparameter settings for the experiments on WILDS.

Dataset	AMAZON	CAMELYON17	CIVILCOMMENTS	FMOW	IWILDCAM	RXRX1
Num. of seeds	3	10	3	3	3	3
Learning rate	2e-6	1e-4	1e-5	1e-4	1e-4	1e-3
Weight decay	0	0	0.01	0	0	1e-5
Scheduler	n/a	n/a	n/a	n/a	n/a	Cosine Warmup
Batch size	64	32	16	32	16	72
Architecture	DistilBert	DenseNet121	DistilBert	DenseNet121	ResNet50	ResNet50
Optimizer	Adam	SGD	Adam	Adam	Adam	Adam
Domains in minibatch	5	3	5	5	10	10
Group by	Countries	Hospitals	Demographics× toxicity	Times × regions	Trap locations	Experimental batches
Training epochs	200	10	5	12	9	90

OOD objective implementations. We choose 4 representative OOD objectives to evaluate the quality of learned features, including GroupDRO (Sagawa* et al., 2020), IRMv1 (Arjovsky et al., 2019), VREx (Krueger et al., 2021) and IRMX (Chen et al., 2022). We implement the OOD objectives based on the code provided by Shi et al. (2022). For each OOD objective, by default, we follow the WILDS practice to sweep the penalty weights from the range of $\{1e-2, 1e-1, 1, 1e1, 1e2\}$, and perform the model and hyperparameter selection via the performance in the provided OOD validation set of each dataset. Due to the overwhelming computational overhead required by large datasets and resource constraints, we tune the penalty weight in iWildCam according to the performance with seed 0, which we empirically find yields similar results as full seed tunning. Besides in Amazon, we adopt the penalty weights tuned from CivilComments since the two datasets share a relatively high similarity, which we empirically find yields similar results as full seed tunning, too. On the other hand, it raises more challenges for feature learning algorithms in iWildCam and Amazon.

Deep Feature Reweighting (DFR) implementations. For the implementation of DFR (Kirichenko et al., 2022; Izmailov et al., 2022), we use the code provided in Izmailov et al. (2022). By default, DFR considers the OOD validation as an unbiased dataset and adopts the OOD validation set to learn a new classifier based on the frozen features from the pre-trained featurizer. We follow the same implementation and evaluation protocol when evaluating feature learning quality in FMoW and CivilComments. However, since Camelyon17 does not have the desired OOD validation set, we follow the "cheating" protocol as in Rosenfeld et al. (2022) to perform the logistic regression based the train and test sets. Note that when "cheating", the model is not able to access the whole test sets. Instead, the logistic regression is conducted on a random split of the concatenated train and test data. Moreover, for Amazon and iWildCam, we find the original implementation fails to converge possibly due to the complexity of the task, and the relatively poor feature learning quality. Hence we implement a new logistic regression based on PyTorch (Paszke et al., 2019) optimized with SGD, and perform DFR using "cheating" protocol based on the OOD validation set and test set. Besides, we find neither the two aforementioned implementations or dataset choices can lead to DFR convergence in RxRx, which we will leave for future investigations.

Feature learning algorithm implementations. We implement all the feature learning methods based on the Fish code framework. For the fairness of comparison, we set all the methods to train the same number of steps or rounds (if applicable) in WILDS datasets. The only exception is in RxRx1, where both Bonsai and FAT require more steps to converge, since the initialized featurizer has a relatively large distance from the desired featurizer in the task. We did not train the model for much too long epochs as Izmailov et al. (2022) find that it only requires $2-5$ epochs for deep nets to learn high-quality invariant features. The final model is selected based on the OOD validation accuracy during the training. Besides, we tune the retain penalty in FAT by searching over $\{1e-2, 1e-1, 0.5, 1, 2, 10\}$, and finalize the retain penalty according to the OOD validation performance. We list the detailed training steps and rounds setups, as well as the used retain penalty in FAT in Table 10.

For ERM, we train the model simply by the overall number of steps, except for RxRx1 where we train the model by $15,000$ steps following previous setups (Shi et al., 2022). Bonsai and FAT directly adopt the setting listed in the Table 10. Besides,

Table 10. Hyperparameter setups of feature learning algorithms for the experiments on WILDS.

Dataset	AMAZON	CAMELYON17	CIVILCOMMENTS	FMOW	IWILDCAM	RXRX1
Overall steps	31,000	10,000	50,445	9,600	48,000	20,000
Approx. epochs	4	10,000	3	4	10	10
Num. of rounds	3	2	3	2	2	10
Steps per round	10,334	5,000	16,815	4,800	10	10
FAT Retain penalty	2.0	1e-2	1e-2	1.0	0.5	10

Bonsai will adopt one additional round for synthesizing the pre-trained models from different rounds. Although Zhang et al. (2022) requires Bonsai to train the two rounds for synthesizing the learned features, we empirically find additional training steps in synthesizing will incur overfitting and worse performance. Moreover, as Bonsai requires propagating $2K-1$ batches of the data that may exceed the memory limits, we use a smaller batch size when training Bonsai in iWildCam (8) and RxRx1 (56).

H.3. Software and hardware

We implement our methods with PyTorch (Paszke et al., 2019). For the software and hardware configurations, we ensure the consistent environments for each datasets. We run all the experiments on Linux servers with NVIDIA V100 graphics cards with CUDA 10.2.